Geo-Bio Interfaces (2025), **2**, e2, 1–16
doi:10.1180/gbi.2024.10

CAMBRIDGE UNIVERSITY PRESS

Article

Speciation-dependent molecular mechanism of electron transfer from the *c*-type cytochrome MtrC to U(VI)-ligand complexes

Margaux Molinas[1], Karin Lederballe Meibom[1], Ashley Brown[1], Luciano A. Abriata[2], Tim Prüßmann[3] and Rizlan Bernier-Latmani[1]

[1]Environmental Microbiology Laboratory, Ecole Polytechnique Fédérale de Lausanne (EPFL), Lausanne, Switzerland; [2]Protein Production and Structure Core Facility, Ecole Polytechnique Fédérale de Lausanne (EPFL), Lausanne, Switzerland and [3]Karlsruhe Institute of Technology (KIT), Institute for Nuclear Waste Disposal (INE), P.O. 3640, D-76021 Karlsruhe, Germany

Abstract

Members of the *Shewanella* genus transfer electrons to metal and actinide electron acceptors such as hexavalent uranium, U(VI), via *c*-type cytochromes. The intracellular mechanism of electron transfer is well studied but the delivery of electrons to external electron acceptors less well so. MtrC, a decaheme *c*-type cytochrome located on the cell surface side of the outer membrane of many *Shewanella* species, and extending to the extracellular medium, transfers electrons to U(VI), both *in vivo* and *in vitro* when purified. However, it is unclear how the electron transfer between the terminal heme(s) of the protein and extracellular U(VI) occurs. In particular, the type of interaction between MtrC and U(VI), and the parameters controlling electron transfer remain to be elucidated. Here, we investigated the kinetics of U(VI) reduction by *S. baltica* MtrC in solution for U(VI) complexed with one of five ligands: carbonate, hydroxyl, citrate, nitrilotriacetic acid (NTA) or ethylenediaminetetraacetic acid (EDTA). We observed two initial reaction rates, one more rapid for U-citrate, U-NTA and U-EDTA, and another slower for U-carbonate and U-hydroxo. By combining Nuclear Magnetic Resonance spectroscopy and M_4-edge High Resolution X-ray Absorption Near Edge Structure spectroscopy, we attributed these differences to the type of interaction between the U-ligand complex and MtrC, *i.e.*, probably electrostatic interaction with the ligand of U-EDTA, hydrogen bonding to the ligand of U-citrate and U-NTA, and covalent bonding with U-carbonate and U-hydroxo. We also demonstrate the persistence of U(V) in the U-carbonate system when interacting with MtrC. Overall, we showed that the mechanism of electron transfer depended on the chemistry of the soluble U(VI) complex serving as the substrate.

Keywords: MtrC; *c*-type cytochrome; electron transfer; reduction kinetics; NMR; HR-XANES

(Received 18 July 2024; revised 24 October 2024; manuscript accepted: 24 November 2024)

Introduction

Uranium is an actinide that is encountered in the environment mainly in two stable oxidation states: U(VI) under oxidized conditions and U(IV) under reduced conditions. The electron transfer allowing U(VI) to be reduced to U(IV) can be performed either abiotically by a wide range of ferrous iron- or sulfide-bearing minerals (O'Loughlin *et al.,* 2003; Scott *et al.,* 2005; Veeramani *et al.,* 2011, 2013), or biologically (Lovley *et al.*, 1991, 1993; Francis *et al.,* 1994; Bargar *et al.,* 2008; Bernier-Latmani *et al.,* 2010). Dissimilatory metal-reducing bacteria are capable of delivering electrons to metals (*e.g.*, Fe or Mn) as well as radionuclides (*e.g.*, U). In particular, *Shewanella oneidensis* MR-1 transfers electrons to U(VI) via *c*-type cytochromes (Marshall *et al.,* 2006). These cytochromes consist of iron (Fe) centres surrounded by a porphyrin ring, known as hemes, embedded in the polypeptide scaffold. The heme Fe centres exist in one of two oxidation states, either reduced Fe(II) or oxidized Fe(III), and electron transfer occurs by switching between these states.

On the cell surface of *Shewanella* species, such as *S. oneidensis* strain MR-1 or *S. baltica* strain OS185, the MtrCAB porin complex embedded in the outer membrane allows electron transfer from the periplasm to the extracellular medium. MtrCAB is composed of the two decaheme *c*-type cytochromes MtrA and MtrC. MtrA faces the inside of the cells, and MtrC is exposed at the surface of the cells. MtrA is inserted inside a β-barrel porin protein MtrB and MtrC sits on the top (Edwards *et al.,* 2020). This porin-complex facilitates electron transfer from the periplasm to the cell surface via direct heme-heme contact between MtrA and MtrC, and MtrC is a terminal reductase that delivers electrons directly to electron acceptors (Marshall *et al.,* 2006; Shi *et al.,* 2006; Hartshorne *et al.,* 2009) (Fig. S1). MtrCAB receives electrons via a chain of *c*-type cytochromes extending to the cytoplasm (Schwalb *et al.,* 2002; Ross *et al.*, 2007; Schuetz *et al.,* 2009; Richardson *et al.*, 2012).

Corresponding Author: Rizlan Bernier-Latmani; Email: rizlan.bernier-latmani@epfl.ch
Cite this article: Molinas M., Lederballe Meibom K., Brown A., Abriata L.A., Prüßmann T., & Bernier-Latmani R. (2025). Speciation-dependent molecular mechanism of electron transfer from the *c*-type cytochrome MtrC to U(VI)-ligand complexes. *Geo-Bio Interfaces* **2**, e2, 1–16. https://doi.org/10.1180/gbi.2024.10

Within the MtrCAB complex, heme 5 of MtrC is oriented towards MtrA and electrons flow from MtrA to MtrC. Three out of ten MtrC hemes are exposed to the extracellular medium (Edwards *et al.,* 2012a, 2015). These are hemes 2, 7 and 10. Heme 2 and 7 are binding sites for a second outer-membrane decaheme *c*-type cytochrome, OmcA (Shi *et al.,* 2006), or binding sites for flavin molecules (Edwards *et al.,* 2012a, 2015; Watanabe *et al.,* 2017) that shuttle electrons to electron acceptors. Heme 10 is expected to be a favourable site for the transfer of electrons to extracellular electron acceptors. In strain MR-1, extracellular electron transfer is the last step of a series of electron transfers along a chain of *c*-type cytochromes and is probably the rate-limiting step in the overall mechanism of electron transfer (White *et al.,* 2013). Several studies have described the electron flow in multiheme *c*-type cytochromes and characterized the process step by step. For instance, scanning tunnelling spectroscopy, which is imaging of a surface at the molecular level by probing with a sharp metallic tip to which a voltage is applied, or its extension, tunnelling spectroscopy (Wigginton *et al.,* 2007a), was applied to measure the conductance of MtrC and OmcA (Wigginton *et al.,* 2007b). In addition, quantum and molecular mechanics were applied to unveil the step-by-step electron transfer in MtrF, a homologue protein to MtrC, giving insights into the redox properties of each heme (Breuer *et al.,* 2014). Furthermore, an alternative method to describing electron transfer within *c*-type cytochromes was derived from the Marcus theory for redox reactions (Pirbadian and El-Naggar, 2012). The Marcus theory describes the parameters which may influence electron transfer during redox reactions and enables the computation of electron tunnelling rates in biological systems; *i.e.*, the rates at which electrons hop from one redox centre to the other (Marcus and Sutin, 1985). These parameters include ΔG^0, the free energy of the reaction, $\Delta G^{\pm}$ the free activation energy, λ the nuclear reorganization energy upon electron transfer, H_{DA} the electronic coupling of the redox couple donor/acceptor, and the temperature.

Yet, it is unclear how electrons are delivered to the electron acceptor. Several types of interactions have been reported between various substrates and *c*-type cytochromes. Motifs have been identified for the binding of MtrC and OmcA to solid iron substrates such as iron oxides (Fe_2O_3) (Lower *et al.,* 2007), and hydrogen interactions invoked as the binding mechanism. In MtrF, a positively charged pocket around heme 6 and 7 was identified and proposed to interact electrostatically with the negatively charged surface of Fe_2O_3 (Fukushima *et al.,* 2017). As for soluble iron substrates, hydrogen bonds were invoked in Fe(III)-citrate and Fe(III)-NTA binding to the undecaheme *c*-type cytochrome UndA of *S. oneidensis* MR-1 (Edwards *et al.,* 2012b). In the case of U, the only evidence of interaction with a *c*-type cytochrome was demonstrated theoretically by density functional theory calculations (Sundararajan *et al.,* 2008). In that study, U(VI) binds covalently to the carboxylic group of an amino acid residue, probably aspartate or glutamate. Based on this limited evidence, the emerging view is that *c*-type cytochromes are versatile proteins that can interact electrostatically, via hydrogen or covalent bonds, with various substrates.

In addition, interactions between electron acceptors and *c*-type cytochromes were evidenced by NMR spectroscopy. In particular, the region of paramagnetically-shifted resonances in ^{1}H-1D NMR spectra is directly sensitive to changes in the chemical and electronic structures of the heme groups. Therefore, perturbations of the signal in the paramagnetic region upon the addition of interacting small molecules can be used to assign binding to specific heme groups. As an example of direct pertinence to our study, ^{1}H-1D NMR spectra of *c*-type cytochromes from *S. oneidensis* MR-1 collected in the presence of various electron acceptors provided information on the interaction between the proteins and their electron acceptor and the specific location of the interaction site (Paquete *et al.,* 2014; Neto *et al.,* 2017; Ferreira and Salgueiro, 2018).

Here, we study the interaction between U(VI) and MtrC from *Shewanella baltica* OS185 (henceforth MtrC baltica) and seek to understand the controls on the electron transfer rate, including the impact of U(VI) speciation. To that end, we chose to investigate a series of environmentally relevant ligands: carbonate, hydroxyl, citrate and the aminocarboxylate compounds nitrilotriacetic acid (NTA), ethylenediaminetetraacetic acid (EDTA) and, for a subset of experiments, diethylenetriaminepentaacetic acid (DTPA) (Fig. S2). The latter three ligands can be used to extract heavy metals and radionuclides from soil (Tandy *et al.,* 2004), due to their chelating properties. We suggest that the type and strength of interaction of MtrC baltica with the U-ligand complexes correlate with the associated rate of reduction and govern the speciation and potential persistence of the U(V) intermediate. The latter contributes to determining the reduction rate. In addition, studying the reduction rate is crucial to understanding the isotopic fractionation behaviour of U in the environment. In fact, different electron transfer rates have been shown to lead to distinct isotope fractionation behaviours (Brown *et al.,* 2023).

Experimental methods

Site directed mutagenesis in MtrC baltica

Plasmid DNA (pBAD-202D TOPO) carrying a gene encoding a soluble version of MtrC, referred to as *mtrCsol* and originating from *Shewanella baltica* OS185, was kindly provided by Marcus Edwards. Five mutants of *mtrCsol* were generated by site-directed mutagenesis. Single point mutations were introduced to mutate the distal histidine (H), bound to the Fe atom of the heme, to a methionine (M). 5'-end phosphorylated primers were designed with the forward ones carrying the point mutations (CAT for histidine substituted by ATG for methionine) (see Table S1 for primer sequences). Individual plasmids containing the five versions of *mtrCsol* were amplified by Polymerase Chain Reaction (PCR) using the phosphorylated primers with Phusion™ Hot Start II DNA Polymerase (ThermoFisher) (Table S2). The resulting linear PCR products were circularized by ligation and transformed into *Escherichia coli* DH10B cells. Plasmids from single colonies were purified and the mutations in the *mtrC* gene were verified by Sanger sequencing (Microsynth) (see Table S3 for primer sequences). The resulting plasmids containing *mtrCsol* with mutations were introduced into *Shewanella oneidensis* MR-1 Δ*OMC* (lacking all outer membrane cytochromes) (Molinas *et al.,* 2023) by electroporation and the presence of plasmids with specific mutations verified by sequencing of re-isolated plasmids.

MtrC purification and reduction

MtrC purification

In addition to MtrC baltica, some experiments were conducted with MtrC originating from *S. oneidensis* MR-1 (hereafter MtrC MR-1). Soluble recombinant protein MtrC MR-1, including a 6xHis tag, was expressed in the double mutant Δ*omcA*Δ*mtrC* strain of *S. oneidensis* MR-1 LS331, kindly provided by Liang Shi. Soluble recombinant protein MtrC baltica was expressed in the double mutant Δ*mtrB*Δ*mtrD* strain *S. oneidensis* MR-1 LS527, kindly provided by Marcus Edwards.

https://doi.org/10.1180/gbi.2024.10 Published online by Cambridge University Press

MtrC MR-1 was purified as previously described (Brown *et al.,* 2023; Molinas *et al.,* 2023). For MtrC baltica, Terrific Broth media (Text S1) containing 30 μg/ml kanamycin was inoculated with 10 mL/L of an overnight culture, grown in LB (prepared from Sigma-Aldrich LB Broth mix) with 30 μg/ml kanamycin at 30°C in a shaking incubator (140 rpm). At an OD_{600} of 0.5, the culture was amended with L-arabinose to a final concentration of 1 mM to induce expression of *mtrC* and incubated overnight at 30°C, shaking at 140 rpm. The supernatant was collected by centrifugation at 6000xg. The supernatant was concentrated to about 100 mL using a Vivaflow®200 cartridge (Sartorius) with a 30 kDa cut-off, connected to a peristaltic pump. The concentrated supernatant was dialyzed against a 20 mM HEPES at pH 7.5 to remove salts. The dialyzed supernatant was loaded onto a Hiprep 16/10 Q column, equilibrated in 20 mM HEPES at pH 7.5, and a salt gradient (0 to 500 mM NaCl) of 30 column volumes was applied in order to elute the protein. Then for either MtrC MR-1 or baltica, the fractions containing soluble MtrC were pooled, concentrated and gel-filtered using a Superdex 200 HiLoad 16/600 column pre-equilibrated with 150 mM NaCl, 20 mM HEPES at pH 7.5. Following elution and concentration, the purified MtrC migrated as a single band on a sodium dodecyl sulfate-polyacrylamide gel electrophoresis (SDS-PAGE) gel with an apparent mass of 75 kDa and 65 kDa for MR-1 and baltica, respectively (Text S2). The concentration was measured by BCA assay (Pierce™ BCA Protein Assay Kits, Thermo Scientific).

The experimental procedure for the purification of the 5 MtrC baltica mutants H208M, H292M, H497M, H643M and H607M follows the same steps as described above for Wild Type MtrC baltica. The purified MtrC baltica mutant proteins migrated as a single band on an SDS-PAGE gel with an apparent mass of 65 kDa (Fig. S3), except for H497M.

MtrC reduction

MtrC reduction was performed in an MBraun glovebox filled with N_2, under the anoxic condition as previously described (Brown *et al.,* 2023; Molinas *et al.*, 2023).

Preparation of the ligand stock solutions

For the organic ligand stock solutions, an appropriate amount of citrate, NTA, EDTA or DTPA was dissolved in a buffer, composed of 100 mM HEPES and 50 mM NaCl at pH 7.5 (buffer A), to a final concentration of 10 mM for citrate and 60 mM for NTA or EDTA. The pH was adjusted to a value of 7.5 using a 10 M NaOH solution. The solutions were either kept oxic for oxic experiments or flushed with N_2 to remove the O_2 and kept under anoxic conditions in an N_2 MBraun glovebox.

For the oxic carbonate stock solution, $NaHCO_3$ salt was dissolved in buffer A to a concentration of 1 M, minimizing the headspace of the stock vial. For the anoxic carbonate stock, the $NaHCO_3$ salt powder was first degassed with N_2, then introduced inside the glovebox and dissolved in buffer A. Equilibration was allowed for 48h.

Kinetics of reduction of U-ligand complexes with MtrC

In the glovebox, working solutions of reduced MtrC baltica or U(VI)-ligand were prepared. The U(VI)-ligand working solutions were prepared by diluting the appropriate volume of an 18 mM uranyl(VI) chloride anoxic stock in the freshly prepared ligand stock solutions. Uranium speciation was modelled using the *Mineql* software (details are provided in the results section). The redox status of MtrC baltica hemes was investigated before the experiments by UV-vis spectroscopy to confirm they were reduced. Equal volumes of the working solutions of reduced MtrC baltica and U(VI)-ligand were mixed so the initial concentration of reduced MtrC baltica and U(VI) were both equal to 100 μM. The sampling consisted of collecting a volume of the reaction mixture after 5s, 15s, 30s and 120s and loading it immediately onto the ion-exchange chromatography resins to separate U(VI) from U(IV) (Molinas *et al.*, 2021, 2023; Brown *et al.,* 2023). U was subsequently measured in each fraction by ICP-MS. The concentration of MtrC baltica was quantified by the BCA assay in the reaction mixture. For each ligand, these reactions were performed in duplicates.

Uranium quantification

Uranium concentration was measured by Inductively Coupled Plasma Mass Spectrometry (ICP-MS 7900, Agilent) for both filtered supernatants and samples eluted from the ion-exchange chromatography test. Dilutions to a range of 1 to 10 ppb of U were performed in a matrix of 1% HNO_3 prior to analysis. All samples were measured in technical duplicates.

^{1}H-1D NMR

NMR experiments were performed at 25°C on a Bruker spectrometer operating at 500 MHz (^{1}H) equipped with a CPTCI cryoprobe and an AvanceNEO-500 console. ^{1}H spectra were acquired with an experiment tailored for the detection of paramagnetically shifted resonances: pre-saturation during a relaxation delay of 0.1s using a hard pulse of around 9 μs and a fast turnover with a total recycle time of 0.33s. FIDs were processed through FFT with 50 Hz of line broadening. All acquisition and data processing were performed with Bruker's *Topspin 4.0*.

Samples of oxidized MtrC baltica with U(VI)-ligand complexes for ^{1}H-1D NMR

Prior to the NMR measurements, the buffer of an aliquot of purified oxic MtrC baltica was exchanged for pure D_2O (pH 7.5) using 30 kDa cut-off centrifugal concentrators (Amicon Ultra-15, Merck Milipore). The concentration of MtrC baltica in the D_2O stock was evaluated by the BCA assay. Identically, a stock of U(VI)-chloride in solution was evaporated and the obtained U(VI)-Cl was dissolved in pure D_2O to a final concentration of 40 mM. Immediately before the measurements, working solutions of oxic MtrC baltica in D_2O and U(VI) in D_2O were prepared. MtrC baltica was diluted to a concentration of 60 μM using 100 mM HEPES and 50 mM NaCl in pure D_2O (pH 7.5). The various U(VI)-ligand solutions were prepared to a concentration of 240 μM U(VI) by diluting the appropriate amount of U(VI)-chloride stock solution in a 60 mM solution of ligand (carbonate, NTA, EDTA, citrate) prepared in 100 mM HEPES and 50 mM NaCl in pure D_2O (pH 7.5). Then, equal volumes of oxic MtrC baltica and U-ligand working solutions were mixed, so that [MtrC baltica] = 30 μM and [U(VI)] = 120 μM. The obtained mixture was placed in an NMR tube.

Samples of MtrC baltica mutants for ^{1}H-1D NMR

Prior to the NMR measurements, the buffer of an aliquot of each of the 5 purified oxic MtrC baltica mutants was exchanged for 100 mM HEPES and 50 mM NaCl in pure D_2O (pH 7.5) using 30 kDa cut-off centrifugal concentrators (Amicon Ultra-15, Merck Milipore). The concentration of MtrC baltica in the D_2O stock was evaluated by BCA assay. 0.5 mL was inserted in an NMR tube and analysed.

https://doi.org/10.1180/gbi.2024.10 Published online by Cambridge University Press

M_4-edge HR-XANES (high energy resolution X-ray absorption near-edge structure) spectroscopy

U(VI)-ligand reacted with reduced MtrC MR-1

Inside a glovebox, equal volumes of a working solution of 1.2 mM of U(VI) in 60 mM ligand (carbonate, NTA or EDTA) and 600 µM of reduced MtrC (MR-1 or baltica) were mixed to initiate the reaction. Consequently, the initial concentrations were 600 µM of U(VI) and 300 µM of MtrC MR-1. Aliquots were collected at distinct time points (carbonate: 30s, 1min, 2min, 5min and 20min; NTA and EDTA: 15s, 30s and 60s) and placed in a –20°C pre-cooled metallic sample holder designed to fit into a N_2-flushed cryostat. The sample holders were sealed anoxically and kept frozen until measured.

Size-exclusion chromatography (SEC) purified mixtures of U(VI)-carbonate and U(VI)-NTA reacted with reduced MtrC baltica for XANES

In order to investigate the oxidation state of U complexes bound to the purified reduced MtrC, we used size-exclusion desalting columns that are ordinarily designed to desalt a protein solution or to exchange a protein buffer. Tests were performed under oxic and anoxic conditions reacting MtrC with five U(VI)-ligand complexes, where the ligands are water (hydroxyl), carbonate, NTA, EDTA and DTPA (concentrations summarized in Table S4). The experimental methods are described in Text S3 and Text S4 for oxic and anoxic conditions respectively, and the results of the tests between MtrC MR-1 and the four U(VI)-ligand complexes carbonate, NTA, EDTA and DTPA are described in Text S5. The amount of U recovered in the fractions under oxic or anoxic conditions is reported in Fig. S4 and Table S5 and Fig. S5 and Table S6, respectively. Moreover, under reduced conditions, U(VI) and U(IV) were separated by IEC for fraction F1 and the combined fractions F2 to F7 (Table S7).

A week ahead of the reaction, the 40 kDa size-exclusion resins (Zeba® Spin Desalting Columns, Thermofisher Scientific) were degassed and introduced into the MBraun glovebox. They were conditioned by 3 washes with buffer A. In the glovebox working solutions of 1.2 mM of U(VI) in 60 mM ligand and of 600 µM reduced MtrC baltica were mixed to initiate the reaction. After 15 minutes, 50 µL were loaded onto the size-exclusion columns and spun for 1.5 min at 3,500xg. The first fraction, containing MtrC baltica, was eluted and 20 µL were directly transferred into a pre-cooled (to –20°C) metallic sample holder designed to fit into a liquid N_2 cryostat. The sample holders were sealed anoxically and kept frozen until measured. U was quantified by ICP-MS.

U M_4-edge XANES

Although three experiments (U(VI)-carbonate with MtrC MR-1, U(VI)-NTA/U(VI)-EDTA with MtrC baltica, and SEC purified U(VI)-carbonate/U(VI)-NTA with MtrC baltica) were performed at different beamtimes, the settings of the beamline were similar for all three.

The U M_4-edge (3.726 keV) HR-XANES was used to elucidate the oxidation state of U in the above-mentioned experiments. Spectra were collected at the station for actinide science (ACT) at the CAT-ACT beamline at the Karlsruhe Institute of Technology Light Source, Karlsruhe, Germany. The CAT-ACT beamline is equipped with a Johann-type X-ray emission spectrometer (Zimina *et al.*, 2017). The incident beam was monochromatized by a Si(111) double crystal monochromator (DCM) and focused onto the sample to a spot size of about 1 mm x 1 mm. The X-ray emission spectrometer consists of four Si(110) crystals with a 1 m bending radius and a single diode VITUS silicon drift detector (Ketek, Germany), which together with the sample are arranged in a vertical Rowland circle geometry. A UO_2 reference was used to calibrate the spectra. The main absorption maximum was set to 3.725 keV. The sample cells were placed in a liquid N_2 cryostat with an insulation vacuum around the sample cells to minimize beam damage while maintaining anoxic conditions. The X-ray spectrometer was inside a He-flushed box in order to minimize intensity loss due to absorption or scattering of photons.

Data processing consisted of normalization and linear combination fitting (LCF) using the ATHENA software (Ravel and Newville, 2005). The spectra obtained were modelled using the references U(VI)-carbonate/U(VI)-NTA, U(V)-iodide and U(IV) O_2, for which spectra were also collected and analysed in the same manner. The goodness of fit was evaluated with two statistical parameters, the R-factor and the reduced χ^2, which were minimized by the fitting algorithm.

Results

All experiments and their corresponding conditions, figures, tables, or descriptions are listed in Table 1.

Kinetics of U(VI) reduction

We investigated the reduction rates of the *c*-type cytochrome MtrC baltica from *S. baltica* OS185 exposed to various U(VI)-ligands complexes to better unravel how U(VI) speciation impacts its reduction.

Reduced MtrC baltica, with all hemes in the Fe^{2+} valence state, was reacted with U bound to the following series of ligands: carbonate, hydroxo, citrate, NTA, EDTA (Fig. 1). The starting ratio of protein to U is reported for each reaction mixture in Table S8, along with their respective concentrations. Experiments with the U(VI)-ligand complexes were performed in duplicate, and the values in Table S8 correspond to the average of the measurements for both experiments. The ratio U:MtrC was adjusted to be close to 1, for consistency across reactions (1.17 ± 0.11 for carbonate, 1.15 ± 0.05 for hydroxo, 1.15 ± 0.06 for citrate, 1.17 ± 0.02 for NTA, 1.24 ± 0.1 for EDTA). Uranium speciation was modelled under the conditions of reaction (100 mM HEPES and 50 mM NaCl, pH 7.5) using the software *Mineql* (Table S9) and applying the thermodynamic data reported in Table S10. The ligand concentration was adjusted to 30 mM so a 1:1 U:ligand complex dominates the speciation with the aminocarboxylate ligands NTA and EDTA. For NTA, the predominant species predicted is the 1:1 U:ligand hydroxo complex, $UO_2(OH)NTA^{2-}$ (97.6%) (Table S9), using thermodynamic values from De Stefano *et al.* (2006). Regarding EDTA, we ran the speciation calculations using two sets of thermodynamic constants. With the logK values published in De Stefano *et al.* (2006), we obtained $UO_2(OH)EDTA^{3-}$ (94.9%) as the dominant species. With thermodynamic data published by Hummel *et al.* (2005), we obtained UO_2EDTA^{2-} as the dominant species (100%) (Table S9). For carbonate, at a concentration of 30 mM, a mixture of the di-carbonato $UO_2(CO_3)_2^{2-}$ (33.3%) and tri-carbonato $UO_2(CO_3)_3^{4-}$ (66.7%) species were observed (Table S9). For citrate at a concentration of 5 mM, of mixture of the mononuclear species UO_2cit^- (73.8%) and of the binuclear species $(UO_2)_2cit_2^{2-}$ (26.2%) is predicted to form (Table S9). The concentration of citrate was set to 5 mM because, under these conditions (100 µM U(VI)), the speciation is independent of the ligand concentration. Finally, according to the

https://doi.org/10.1180/gbi.2024.10 Published online by Cambridge University Press

Table 1. List of experiments and corresponding figures, tables, or supplementary texts.

Experiment	Figure(s)/table(s)/text(s)	Experimental conditions
Minelq modelling of U-ligand complexes	Fig. S2, Table S9, Table S10	[U(VI)] = 100 μM [ligand] = 30 mM, [citrate] = 5 mM pH 7.5, 100 mM HEPES and 50 mM NaCl
Kinetics of reduction U(VI)-ligand complexes by reduced MtrC baltica	Fig. 1, Fig. 2, Table S8	[U(VI)] = 100 μM [reduced MtrC baltica] = 100 μM [ligand] = 30 mM, [citrate] = 5 mM pH 7.5, 100 mM HEPES and 50 mM NaCl
Kinetics of reduction of U(VI)-ligand complexes by reduced MtrC MR–1	Fig. S9, Fig. S10	[U(VI)] = 100 μM [reduced MtrC MR–1] = 100 μM [ligand] = 30 mM pH 7.5, 100 mM HEPES and 50 mM NaCl
Purification of MtrC baltica point mutation mutants	Fig. S3, Table S1, Table S2, Table S3	pH 7.5, 20 mM HEPES, 150 mM NaCl
NMR on MtrC baltica mutants	Fig. 3, Fig. S6	[oxidized MtrC baltica mutants] = 30 μM pH 7.5, 100 mM HEPES and 50 mM NaCl
NMR on oxidized form of MtrC baltica reacted with U(VI)-ligand complexes	Fig. 4, Fig S7	[U(VI)] = 120 μM [oxidized MtrC baltica] = 30 μM [ligand] = 30 mM, [citrate] = 5 mM pH 7.5, 100 mM HEPES and 50 mM NaCl
SEC chromatography on MtrC MR–1 reacted with U(VI)-ligand complexes in oxic and anoxic conditions	Text S3, Text S4 Text S5, Fig. S4, Fig. S5, Table S4, Table S5, Table S6, Table S7	[U(VI)] = 150 μM [oxidized/reduced MtrC baltica] = 150 μM [ligand] = 30 mM pH 7.5, 100 mM HEPES and 50 mM NaCl
HR-XANES on reduced MtrC MR–1 reacted with U(VI)-carbonate	Text S7, Fig. 5 and Fig. S11, Table S11 and Table S12.A	[U(VI)] = 600 μM [reduced MtrC MR–1] = 300 μM [carbonate] = 30 mM pH 7.5, 100 mM HEPES and 50 mM NaCl
HR-XANES on SEC treated reaction mixture of reduced MtrC baltica reacted with U(VI)-carbonate	Text S7, Fig. 6, Table S12.D, Table S13	[U(VI)] = 600 μM [reduced MtrC baltica] = 300 μM [carbonate] = 30 mM pH 7.5, 100 mM HEPES and 50 mM NaCl
HR-XANES on reduced MtrC baltica reacted with U(VI)-NTA	Text S7, Fig. 7 and Fig.S13, Table S12.B, Table S14	[U(VI)] = 600 μM [reduced MtrC baltica] = 300 μM [NTA] = 30 mM pH 7.5, 100 mM HEPES and 50 mM NaCl
HR-XANES on reduced MtrC baltica reacted with U(VI)-EDTA	Text S7, Fig. S12 and Fig. S14, Table S12.C and Table S14	[U(VI)] = 600 μM [reduced MtrC baltica] = 300 μM [EDTA] = 30 mM pH 7.5, 100 mM HEPES and 50 mM NaCl

latest updates of the thermodynamic database (Palmer *et al.,* 2003), the dominant hydroxo complex predicted is $UO_2(OH)_3^-$ (99.8%) (Table S9).

Once the reactions between reduced MtrC and the abovementioned complexes were initiated, four time points were taken at 5 s, 15 s, 30 s and 120 s, and analysed for the U oxidation state to resolve the rate of reduction (Fig. 1). The U oxidation state was determined by ion-exchange chromatography as reported in previous work (Molinas *et al.,* 2021, 2023; Brown *et al.,* 2023), allowing separation of U(VI) from U(IV) via an anionic exchange column. Three phases were identified, and second-order kinetic models were used to describe the two first phases: phase 1 from 0 s to 5 s and phase 2 from 5 s to 30 s (Figs 1 and 2). The kinetic constants for each reaction were extracted from the slope of the regression line (Tables in Fig. 2). Interestingly, we noticed two groups of reaction rates in the first 5 s of the reaction (Fig. 2a). On the one hand, complexes of U(VI) with citrate, NTA and EDTA presented very rapid reaction rates, with kinetics constants of $0.0019\%^{-1}.s^{-1}$, $0.0022\%^{-1}.s^{-1}$ and $0.0027\%^{-1}.s^{-1}$ respectively (Table in Fig. 2a). The reaction reached 48.9%, 52.8% and 57.2% of completion, respectively, within 5s. On the other hand, complexes of U(VI) with carbonate and hydroxyl were reduced at slower rates, with 2nd order kinetics constants of $0.0003\%^{-1}.s^{-1}$ and $0.0002\%^{-1}.s^{-1}$, respectively (Table in Fig. 2a). The reactions displayed 12.4% and 9.9% reduction after 5s, respectively.

From 5 s to 30 s (Fig. 1), three different behaviours were observed. Indeed, U(VI)-EDTA reduction is the fastest with a reduction rate of $0.0019\%^{-1}.s^{-1}$, followed by U(VI)-NTA with a reduction rate of $0.0002\%^{-1}.s^{-1}$ (Table in Fig. 2b). The complexes of U(VI) with carbonate, hydroxo and citrate have comparable slower reduction rates, $0.00003\%^{-1}.s^{-1}$, $0.00007\%^{-1}.s^{-1}$ and $0.00008\%^{-1}.s^{-1}$, respectively.

After 30s, the reduction rate is slower for all U(VI)-ligand complexes. The kinetics constants follow a similar order compared to that observed from 5 s to 30 s.

We conclude here that the reduction rate depends on the U-ligand complex chemical characteristics. Four overall behaviours were identified over the 120s reaction time: (i) slow for carbonate and hydroxo, (ii) initially fast then slow for citrate, (iii) initially fast then moderate for NTA and (iv) fast for EDTA. In particular, the

https://doi.org/10.1180/gbi.2024.10 Published online by Cambridge University Press

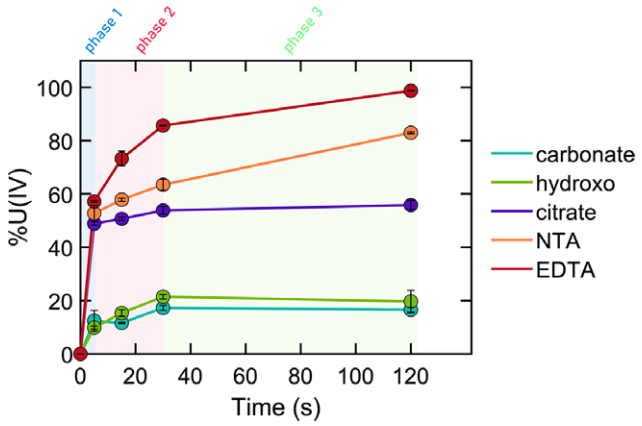

Figure 1. Redox reactions between reduced MtrC baltica and U(VI)-carbonate (turquoise), U(VI)-hydroxo (green), U(VI)-citrate (purple), U(VI)-NTA (orange) and U(VI)-EDTA (red). Time points were obtained at 5s, 15s, 30s and 120s. Reaction progress is characterized by the percentage of the reduction product U(IV) (%U(IV) reported on the y-axis) formed over time, determined by ion exchange chromatography. Ion exchange chromatography allows the separation of U(VI) and U(IV) oxidation states. The concentrations of reactants were: [U(VI)] = 100 μM and [MtrC baltica] = 100 μM. Ligand concentrations are the following: [carbonate] = [NTA] = [EDTA] = 30 mM and [citrate] = 5 mM. For the U(VI) hydroxo complexes, the ligands are hydroxyl groups (Table S9 and S10). The buffer contained [NaCl] = 50 mM and [HEPES] = 100 mM at pH 7.5. Three phases were identified to describe the reaction kinetics, a first phase (blue), second phase (red) and third phase (green).

initial rates of reduction of U(VI)-carbonate and U(VI)-hydroxo complexes were an order of magnitude lower compared to those of U(VI)-citrate, U(VI)-NTA and U(VI)-EDTA.

Localization of MtrC baltica heme groups by ^{1}H NMR spectroscopy

The region spanning 14 to 35 ppm of the ^{1}H-1D-NMR spectrum of MtrC baltica displays the paramagnetically shifted signals arising from H atoms of the heme groups in their Fe(III) form, reporting directly on the geometric and electronic structures around these atoms. We sought to localize the heme groups most likely to engage in an interaction with electron acceptors. To that end, we first designed 5 mutants of MtrC baltica wild type, each mutant harbouring a single mutation (histidine (H) to methionine (M)) in close vicinity to a specific heme: H208M (heme 2), H292M (heme 5), H497M (heme 7), H643M (heme 9) and H607M (heme 10). Such a mutation results in the alteration of the local chemistry around the heme, allowing the assignment of specific regions of the ^{1}H-1D-NMR spectra to individual hemes, as done by Neto *et al.* (2017). Spectra for mutants of heme 2, 5, 9 and 10 are displayed in Fig. 3, and that of the mutant of heme 7 is shown in Fig. S6. Compared to other mutants, MtrC H497M (heme 7) migrated on the SDS-page gel as a sharp band with a size of around 30 kDa, instead of 64 kDa, where a minor band was observed (Fig. S3). The protein might be

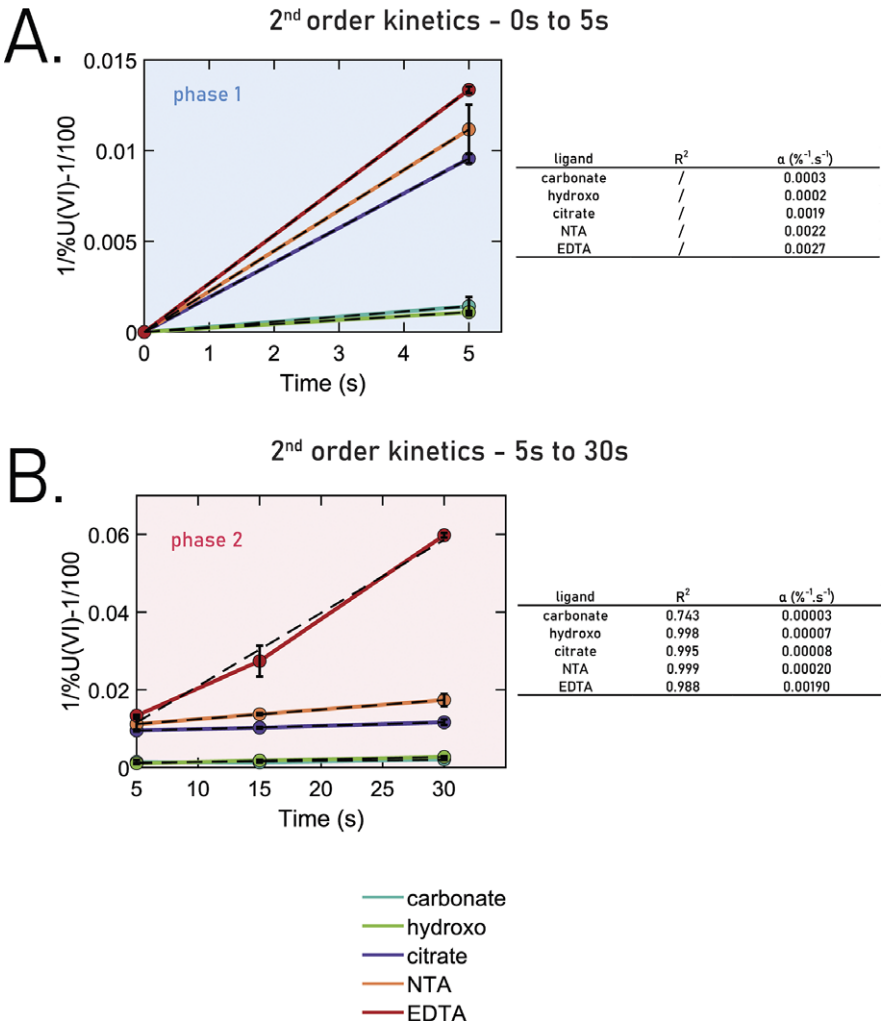

Figure 2. Second order kinetics fitted to the two first phases observed in the reactions described in Fig. 1 between reduced MtrC baltica and U(VI)-carbonate (turquoise), U(VI)-hydroxo (green), U(VI)-citrate (purple), U(VI)-NTA (orange) and U(VI)-EDTA (red): (a) 0 s to 5 s; (b). 5 s to 30 s. The linear regression for each U-ligand complex is displayed in a dotted black line, along with R^2 and the coefficient α of the regression line, corresponding to the kinetic constant of these reactions.

https://doi.org/10.1180/gbi.2024.10 Published online by Cambridge University Press

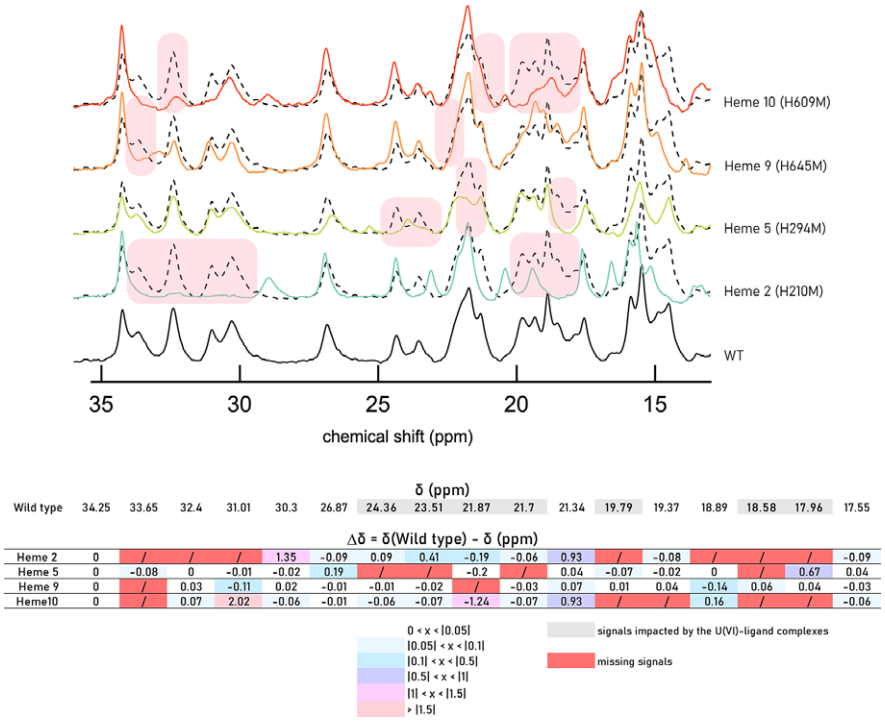

δ (ppm)

Wild type	34.25	33.65	32.4	31.01	30.3	26.87	24.36	23.51	21.87	21.7	21.34	19.79	19.37	18.89	18.58	17.96	17.55

Δδ = δ(Wild type) - δ (ppm)

Heme 2	0	/	/	/	1.35	-0.09	0.09	0.41	-0.19	-0.06	0.93	/	-0.08	/	/	/	-0.09
Heme 5	0	-0.08	0	-0.01	-0.02	0.19	/	/	-0.2	/	0.04	-0.07	-0.02	0	/	0.67	0.04
Heme 9	0	/	0.03	-0.11	0.02	-0.01	-0.01	-0.02	/	-0.03	0.07	0.01	0.04	-0.14	0.06	0.04	-0.03
Heme10	0	/	0.07	2.02	-0.06	-0.01	-0.06	-0.07	-1.24	-0.07	0.93	/	/	0.16	/	/	-0.06

0 < x < |0.05|
|0.05| < x < |0.1|
|0.1| < x < |0.5|
|0.5| < x < |1|
|1| < x < |1.5|
> |1.5|

signals impacted by the U(VI)-ligand complexes
missing signals

Figure 3. Paramagnetic region of the ^{1}H-1D-NMR spectra of oxidized MtrC baltica and mutants H208M, H292M, H643M and H607M. The mutations correspond to the replacement of an axial histidine bound to the hemic iron by a methionine for hemes 2, 5, 9 and 10, respectively. The spectra of wild-type oxidized MtrC baltica is displayed in black at the bottom of the graph and as a dotted line along with the spectra of those of MtrC baltica mutants to clarify the impact of the mutation on the local chemistry of the hemes. Observed shifts or missing resonances are highlighted on the graph in light pink. The table below the figure summarizes the chemical shifts observed for MtrC baltica wild type and the four mutants. The chemical shifts highlighted in grey correspond to signals which appeared to be perturbed upon the interaction of oxidized MtrC baltica and the U(VI)-ligand complexes. The bottom part of the table reports Δδ between the signals of the MtrC wild-type and that of the mutants. The colour code indicates the magnitude of Δδ as described in the legend below the table. The minimum threshold for a relevant shift was set to |0.05| ppm. Hence, the highlighted Δδ values evidence regions where chemical interactions may take place.
The chemical shifts in red in cells marked with / indicate that a signal corresponding to a specific chemical shift in the wild-type spectrum could not be identified in the mutant spectrum.

sensitive to gel migration, partly degraded, or the mutation has perturbed the proper folding or structural organization of MtrC H497M. Hence for completeness, we retained MtrC H497M in the SI, but we will not consider it further nor draw any conclusion from the observed NMR spectrum (Fig. S6).

The NMR spectra of the four mutants shown in Fig. 3 clearly display peak shifts and changes in the paramagnetic region compared to that of the MtrC baltica wild type. These perturbations in the NMR signals are reported in the Table of Fig. 3. MtrC H208M (heme 2) lacks peaks in the 17 ppm – 21 ppm region at 17.96 ppm, 18.58 ppm, 18.89 pm and 19.79 ppm, and also in the 30 ppm – 34 ppm region at 31.01 ppm, 32.4 and 33.65 ppm, pointing that those were related to the chemistry around heme 2 (Table in Fig. 3). As for MtrC H292M (heme5), the resonance at 18.58 ppm is missing, and the region between 21.5 ppm – 25 ppm is affected by the mutation with missing peaks at 21.7 ppm, 23.51 ppm and 24.36 ppm (Table of Fig. 3). MtrC H643M (heme 9) lacks the peaks at about 21.87 ppm and 33.65 ppm (Table in Fig. 3). Finally, the MtrC H607M (heme 10) spectrum displays changes in the region from 17 ppm – 20 ppm with resonances missing at 17.96 ppm, 18.58 ppm 19.37 ppm and 19.79 ppm, as well as in the 30 ppm – 35 ppm region at 33.65 ppm (Table in Fig. 3).

NMR of MtrC incubated with U-ligand complexes

Paramagnetically shifted NMR resonances from heme H atoms also serve to investigate protein-ligand interactions (Paquete *et al.*, 2014; Neto *et al.*, 2017; Ferreira and Salgueiro, 2018). We collected ^{1}H NMR spectra of oxidized MtrC baltica incubated with selected U(VI)-ligand complexes and investigated which NMR resonances changed upon ligand addition. The information was interpreted based on the assignment of heme signals achieved above by collecting NMR spectra of the mutant proteins. Potential interactions between MtrC baltica and the U(VI)-ligand complexes are expected to manifest through peak shifts in the corresponding spectra compared to the reference U-free MtrC baltica. Meaningful perturbations were attributed to chemical shifts variations above a set threshold of 0.05 ppm, which corresponds to twice the threshold used in a previous study (Paquete *et al.*, 2014), in order to minimize uncertainty and focus on the salient features of the interaction between U complexes and MtrC baltica.

Spectra were collected on mixtures of 30 μM of oxidized MtrC baltica and 120 μM U(VI) in the appropriate ligand solution: 30 mM carbonate, 5 mM citrate, 30 mM NTA or 30 mM EDTA (Fig. 4 and Fig. S7). The variations in chemical shifts Δδ between the unreacted MtrC baltica spectrum and those from the various reaction mixtures are reported in the table in Fig. 4.

As a control, for each of the five ligands, a mixture of oxidized MtrC baltica and the ligand solution (same concentration as above) lacking U was investigated to probe the potential impact of the ligand itself on the MtrC baltica NMR signal. In addition, to verify the impact of the ionic strength of the medium on the MtrC baltica NMR signals, oxidized MtrC baltica mixed with 90 mM NaCl was studied (Fig. 4). A split of the main peak at 21.7 ppm, and a slight shift of two peaks at 23.51 ppm and 24.367 ppm were observed with 40 mM additional NaCl (90 mM total) compared to MtrC baltica with the buffer (Table in Fig. 4). This observation suggests that the ionic strength of the solution impacts the above-mentioned signals.

When incubated with U(VI)-hydroxo, four significant peak shifts were observed at 17.96 ppm, 18.58 ppm, 21.87 ppm and 23.51 ppm, suggesting that the complex interacts with MtrC baltica (Table in Fig. 4).

For the carbonate system, the ligand alone provoked peak shifts at 18.58 ppm, 19.79 ppm, 21.7 ppm, 21.87 ppm and 23.51 ppm. However, the amendment of U(VI)-carbonate led to a stronger splitting of the peak at 21.7 ppm, a larger shift at 18.58 ppm and an additional shift at 24.36 ppm (Fig. 4). Hence here the addition of U, induced additional perturbations compared to that of the carbonate ligand alone.

Regarding the citrate system, the ligand-only condition induced shifts and splits of peaks in the region between 17 ppm – 19 ppm at

https://doi.org/10.1180/gbi.2024.10 Published online by Cambridge University Press

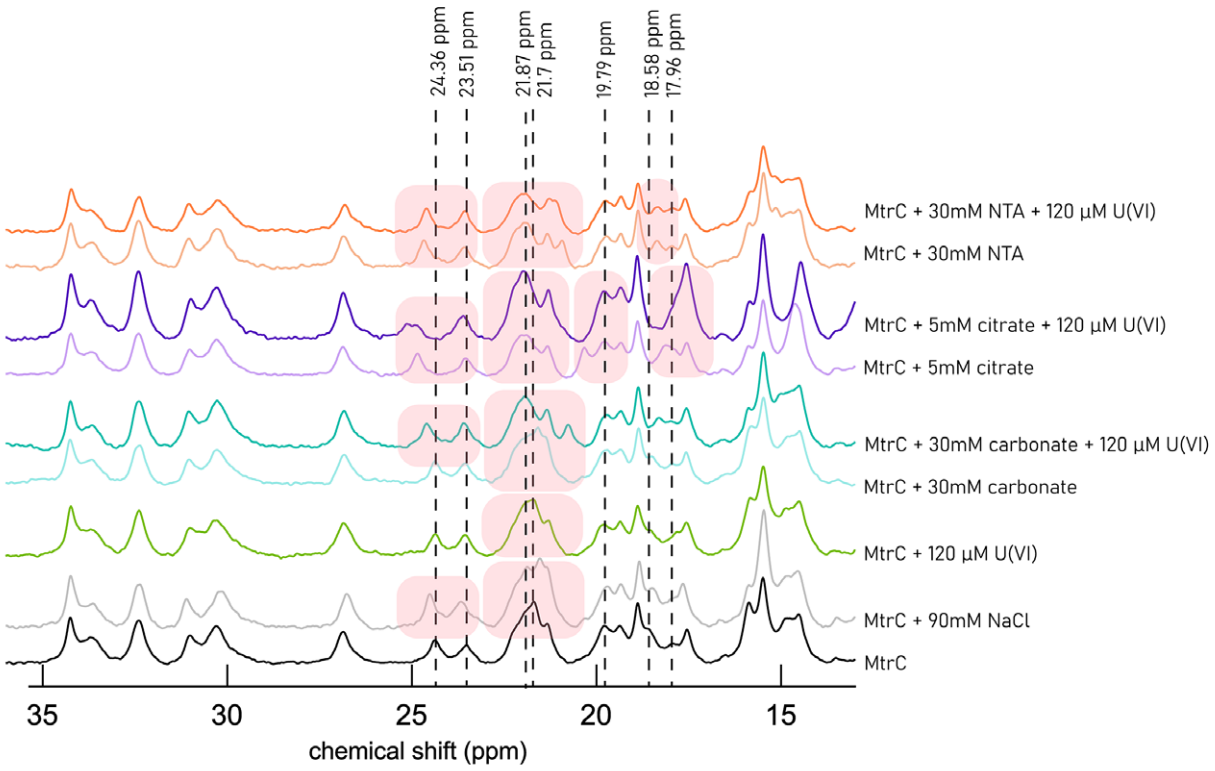

	δ (ppm)																
MtrC	34.25	33.65	32.4	31.01	30.3	26.87	24.36	23.51	21.87	21.7	21.34	19.79	19.37	18.89	18.58	17.96	17.55
	Δδ = δ(MtrC) - δ (ppm)																
90mM NaCl	0.000	0	0	-0.09	0.12	0.11	-0.17	-0.15	0	0.18	0	0.08	0	0.05	0.08	0	-0.11
120µM U(VI)-hydroxo	0.000	-0.02	0	0.01	-0.03	0.02	-0.01	-0.06	-0.05	0	0.04	-0.04	0	0	0.05	0.15	0
30mM carbonate	0.000	-0.03	0.03	-0.04	0.01	0.03	-0.03	-0.06	-0.17	0.11	-0.04	0.05	0.03	0.02	0.07	0	-0.02
120 µM U(VI)-carbonate	0.000	-0.01	-0.01	-0.05	0.03	0.02	-0.25	-0.08	-0.08	0.94	0	0.06	0.03	0.02	0.26	-0.04	-0.02
5mM citrate	0.000	0	0	-0.01	0.02	0	-0.49	-0.04	-0.11	1.37	0.02	0.01	0.03	0	0.44	0.07	0
120 µM U(VI)-citrate	0.000	-0.03	-0.01	0.03	0.01	0.01	-0.53	-0.1	-0.11	2.8	0.03	0	0.02	0	0.59	0.11	-0.01
30mM NTA	0.010	-0.03	0	-0.03	0.03	0.01	-0.31	-0.07	-0.04	0.77	0.01	0.07	0.03	0.02	0.22	0.01	-0.04
120 µM U(VI)-NTA	0.020	-0.05	0.01	-0.02	0.03	0.05	-0.25	-0.05	-0.04	0.59	0.06	0.03	0.03	0.01	0.24	0	-0.03

0 < x < |0.05|
|0.05| < x < |0.1|
|0.1| < x < |0.15|
|0.15| < x < |0.2|
> |0.2|

Figure 4. Paramagnetic region of the ^{1}H-1D-NMR spectra of oxidized MtrC baltica exposed to U-ligand complexes or ligands in a buffer containing [NaCl] = 50 mM and [HEPES] = 100 mM at pH 7.5. NMR was used to decipher potential chemical interactions between U-ligand complexes and oxidized MtrC. Eight reaction mixtures, described on the right-hand side of the graph, were investigated. For each U-ligand complex, spectra of the mixture between ligand alone and oxidized MtrC baltica were recorded for reference. The spectra of MtrC baltica (black) correspond to the reference against which other conditions are evaluated for peak shifts. The spectra of MtrC baltica in 90 mM NaCl (grey) reflect how ionic strength may impact chemical shifts of MtrC baltica spectra. Observed shifts are highlighted on the graph in light pink and chemical shifts of these events are reported on the top of the graph and marked with a dotted black line.
The table below the figure summarizes the chemical shifts observed for MtrC baltica (first line). The chemical shifts highlighted in grey correspond to signals which appeared to be perturbed upon the interaction of oxidized MtrC baltica and the U(VI)-ligand complexes. The bottom part of the table reports Δδ between the signals of MtrC and that of the reaction mixture in the presence of the various ligands and U(VI)-ligand complexes. The colour code indicates the magnitude of Δδ as described in the legend below the table. The threshold for a relevant shift was set to |0.05| ppm and above. Hence, the highlighted Δδ values evidence regions where chemical interactions may take place.

17.96 ppm and 18.58 ppm, respectively, and in the region 21 ppm – 25 ppm at 21.7 ppm, 21.87 ppm and 24.36 ppm, respectively. When U(VI) was added, larger shifts were observed at 18.58 ppm, 21.7 ppm and 24.36 ppm, and an additional shift at 23.51 ppm (Fig. 4). Thus, the addition of U had an impact on the perturbation of the NMR signal caused by the ligand alone.

With NTA, shifts at 18.58 ppm, 21.7 ppm, 21.87 ppm and 24.36 ppm were observed. The addition of U(VI)-NTA did not result in further perturbation, suggesting that U does not interact directly with the protein in the vicinity of the MtrC baltica hemes (Table of Fig. 4).

Finally, as for NTA, EDTA induced a shift at 18.58 ppm, 19.79 ppm, 21.7 ppm, 23.51 ppm and 24.36 ppm (Table of Fig. S7). However, the addition of U(VI)-EDTA did not further impact the NMR signal (Table of Fig. S7).

Overall, the addition of U(VI), ligand, or U(VI)-ligand complexes impacts defined signals or groups of signals of the paramagnetic region of MtrC baltica's NMR spectrum. Indeed, we observed

https://doi.org/10.1180/gbi.2024.10 Published online by Cambridge University Press

that for U(VI)-carbonate and U(VI)-citrate, the addition of U(VI) further alters the heme signature relative to that obtained with the ligand alone. As for the aminocarboxylate ligands, NTA and EDTA, the ligand itself seems to significantly impact the NMR signals, however, the addition of U(VI) does not induce additional changes.

U speciation determined by M_4-edge HR-XANES

Due to technical difficulties, M_4-edge HR-XANES data were acquired with MtrC MR-1 for the carbonate system, while for others (NTA and EDTA), MtrC baltica was used. MtrC MR-1 and MtrC baltica are both decaheme c-type cytochromes and function as terminal reductases at the cell surface of *Shewanella* species. They share 46.6% of identity (Text S6), and the main structural regions are conserved across the two proteins. In particular, the 4 characteristic domains, two beta-barrels and two alpha-helix domains, overlap (Edwards *et al.,* 2015, 2020) (Fig. S8). In addition, the heme chains inside the protein scaffolds align perfectly (Fig. S8). Kinetics of reduction showed similar features when MtrC MR-1 (Fig. S9 and S10) or MtrC baltica (Fig. 1 and 2) were incubated with U(VI)-ligand complexes where the ligand was either carbonate, citrate, NTA, EDTA or DTPA. Hence, we expect that the observations from the M_4-edge spectra for MtrC MR-1 with U(VI)-carbonate can be extended to the reaction between MtrC baltica and U(VI)-carbonate.

U speciation during reaction of U(VI)-carbonate with reduced MtrC MR-1

U(VI)-carbonate was reacted with reduced MtrC MR-1 and the progress of the reaction measured after 30 s, 1 min, 2 min, 5 min and 20 min of reaction using ion-exchange chromatography (Table S11) and M_4-edge HR-XANES spectroscopy (Fig. 5). The former does not resolve U(V) and provides an indication of the progress of the reduction. In contrast, M_4-edge HR-XANES provides direct evidence of U(V). Over time, the spectra shifted to lower energies, towards the U(IV)O_2 standard white line (Fig. 5, Table S12.a), consistent with the ion-exchange chromatography results. These spectra were fitted using linear combination fitting (LCF) (Fig. 5) with U(VI)-carbonate, U(IV)O_2 and U(V)-iodide (a proxy for U(V) species) as references. The fits revealed the persistence of U(V) as 52.97 ± 0.04% U(V) and 42.92 ± 0.02% U(IV) were obtained for the 30 s timepoint, and 33.4 ± 0.01% U(V) and 64.1 ± 0.01% U(IV) at 20 min (Fig. 5). Moreover, we ensured that the fits were robust by comparing them to a model that uses only U(VI) and U(IV) as references and established that the presence of U(V) as a reference yields a vastly better fit (Fig. S10 and Text S7).

To investigate the amount and speciation of U associated with the protein, the reaction mixture was purified after ~15 min using SEC to separate the protein from the aqueous phase and ~9% of the total U was found to be bound to MtrC baltica (Table S13.b). In addition, ion-exchange chromatography of the entire sample reports among the 80% of reduced species, 52.8% of U is in U(IV) form after 16.5 min (Table S13.a). We used M_4-edge HR-XANES spectroscopy to determine the U oxidation state of protein-associated U (Fig. 6). The white line of the spectrum is at 3.72719 keV, close to that of U(VI) (Table S12.d). However, the feature indicated by a black arrow in Fig. 6 at 3.72625 keV infers the presence of reduced oxidation states. The best fit was obtained with all three references, yielding 18.8 ± 0.01% U(VI), 40.18 ± 0.02% U(V) and 41.01 ± 0.02% U(IV) (Table in Fig. 6). Thus, U(V) is a significant contributor to the speciation of protein-associated U.

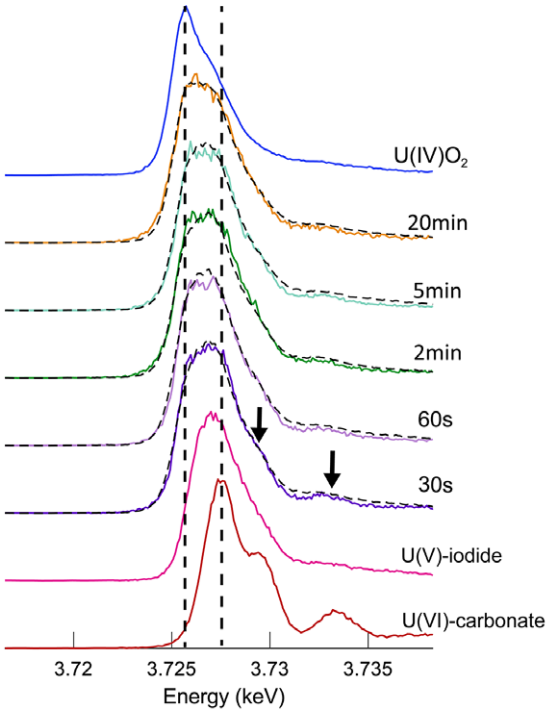

	% U(VI)	% U(V)	% U(IV)	R factor	Reduced χ^2
30s	4.11 ± 0.01	52.97 ± 0.04	42.92 ± 0.02	0.0061	0.0895
1min	1.89 ± 0.01	51.24 ± 0.04	46.87 ± 0.03	0.0059	0.0953
2min	6.51 ± 0.0	40.80 ± 0.00	52.69 ± 0.0	0.0059	0.0855
5min	0.17 ± 0.0	52.18 ± 0.01	47.65 ± 0.01	0.0078	0.1163
20min	2.47 ± 0.0	33.39 ± 0.01	64.14 ± 0.01	0.0058	0.0754

Figure 5. M_4-edge HR-XANES spectra of the reaction between reduced MtrC MR-1 and U(VI)-carbonate as a function of time. The concentrations of reactants were: [U(VI)] = 600 μM and [MtrC MR-1] = 300 μM in a buffer containing [carbonate] = 30 mM, [NaCl] = 50 mM and [HEPES] = 100 mM at pH 7.5. Timepoints were taken after 30 s (purple), 60 s (lavender), 2 min (dark green), 5 min (turquoise) and 20 min (clementine). The reference spectra used to interpret the data are U(VI)-carbonate (red), U(V)-iodine (pink) and U(IV)O_2 (blue). The two dotted lines correspond to the whitelines of U(IV)O_2 on the left, and that of U(VI)-carbonate on the right. Whitelines of the spectra are reported in Table S12.a. LCF fits are displayed as dotted black lines on the top of the M_4-edge HR-XANES spectra obtained. The fits were obtained by considering contributions from U(VI)-carbonate, U(V)-iodide and U(IV)O_2. The black arrows point at spectral features associated with U(V) reduced species. Statistical parameters and results of the fit are summarized in the table below the figure.

U speciation during reaction of U(VI)-NTA or U(VI)-EDTA with reduced MtrC baltica

U(VI)-NTA and U(VI)-EDTA were reacted with reduced MtrC baltica and the U speciation measured after 15 s, 30 s and 60 s using M_4-edge HR-XANES spectroscopy (Fig. 7 for U(VI)-NTA, and Fig. S12 for U(VI)-EDTA). The progression of the reaction was also followed by ion-exchange chromatography Table S14.

For U(VI)-NTA, the LCF fit with three references, U(VI)-NTA, U(V)-iodide and U(IV)O_2, resulting in 51.58 ± 0.03% U(V) and 28.76 ± 0.01% U(IV) at 15s (Fig. 7) and 51.07 ± 0.03% U(V) and 34.34 ± 0.01% U(IV) at 60 s (Fig. 7), suggesting that reduction proceeds slowly for these timepoints as observed with the kinetics data (Fig. 1 and Fig. 2). This suggests that U(V)-NTA may form transiently during the reduction of U(VI)-NTA by reduced MtrC baltica. The spectrum obtained for the 30 s timepoint is noisier because of technical difficulties encountered at the beamline. The fit provided is not statically as robust as those of the 15 s and 60 s timepoints (Table in Fig. 7), hence we will not draw conclusions regarding this result.

https://doi.org/10.1180/gbi.2024.10 Published online by Cambridge University Press

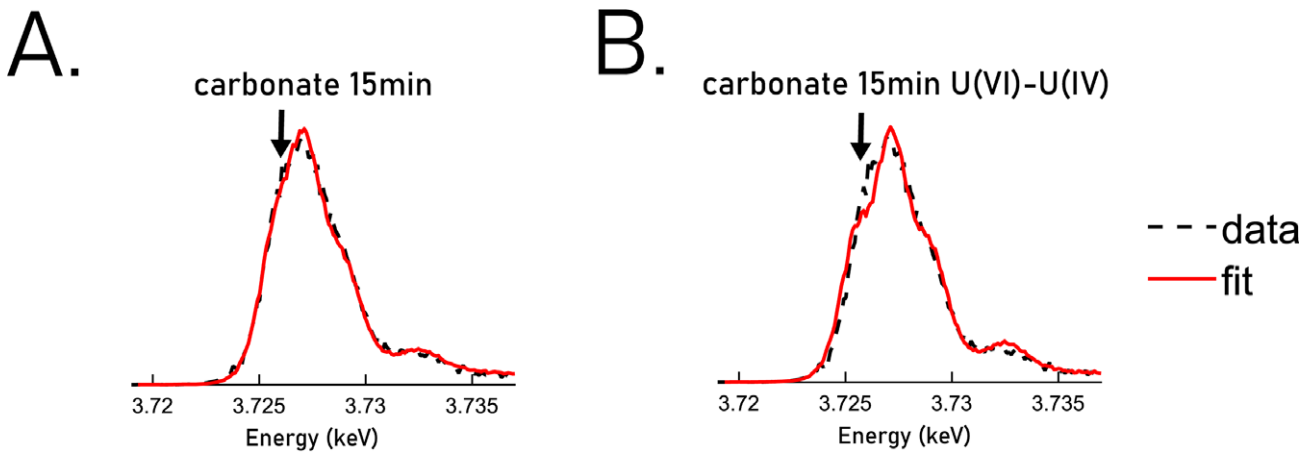

	% U(VI)	% U(V)	% U(IV)	R factor	Reduced χ^2
carbonate 15min	18.8 ± 0.01	40.18 ± 0.02	41.01 ± 0.02	0.0051	0.7470
carbonate 15min U(VI)-U(IV)	29.98 ± 0.01	/	70.02 ± 0.014	0.0153	2.2419

Figure 6. LCF fitting results (red) compared to the data (dotted black) for the M_4-edge HR-XANES spectra obtained on the SEC purified mixture after 15 min of reaction between 300 μM reduced MtrC baltica and 600 μM U(VI)-carbonate at pH 7.5. The fits were obtained by considering contributions from U(VI)-carbonate, U(V)-iodide and U(IV)O_2 (a), or contributions from U(VI)-carbonate and U(IV)O_2 (b). The black arrows indicate presence of reduced species. Statistical parameters and results of the fit are summarized in the table below the figures.

Similarly to the U(VI)-carbonate system, we probed the amount and speciation of protein-associated U. While 97.7% of U was in U(IV) form after 16.5 min (Table S13.a), only 0.36% of the total U was bound to MtrC baltica (Table S13.b).

Interestingly, for the EDTA system, 81.43% U(IV), which corresponds to about 90% of reduced species in case U(V) is also present, was obtained by ion-exchange chromatography after 2.5 min of reduction (Table S14). These data are confirmed by spectroscopic results only when the U(V) reference is included in the model. Indeed, after 60 s, we observed 23.28 ± 0.04% U(VI), 59.18 ± 0.05% U(V) and 17.54 ± 0.02% U(IV) (Fig. S12), totalling about 80% of reduced species. For both the U-NTA and U-EDTA systems, the transient formation of U(V) could account for the data observed.

The fits obtained for U-NTA and U-EDTA systems were compared to a model that uses only U(VI) and U(IV) as references and established that the presence of U(V) as a reference provides a better fit (Fig. S13, Fig. S14 and Text S7).

Discussion

We investigated the reduction mechanism of various U(VI)-complexes by the *c*-type cytochrome MtrC from *Shewanella* species. We combined reduction kinetics, NMR spectroscopy and M_4-edge HR-XANES spectroscopy to get insights into the molecular mechanism of electron transfer and to identify factors controlling the electron transfer rate.

The reduction kinetics results showed that the reduction rate of U(VI) by MtrC depends greatly on its speciation (Fig. 1). Complexes such as U(VI)-carbonate or U(VI)-hydroxo displayed slower initial (0 to 5s) reduction rates ($0.0003\%^{-1}.s^{-1}$ and $0.0002\%^{-1}.s^{-1}$, respectively) than U(VI)-citrate, U(VI)-NTA or U(VI)-EDTA ($0.0019\%^{-1}.s^{-1}$, $0.0022\%^{-1}.s^{-1}$ and $0.0027\%^{-1}.s^{-1}$) (Fig. 2a). In the following step of the reaction, the U(VI)-EDTA reduction rate ($0.0019\%^{-1}.s^{-1}$) was 3 orders of magnitude higher than those of U(VI)-carbonate ($0.00003\%^{-1}.s^{-1}$), hydroxo ($0.00007\%^{-1}.s^{-1}$), citrate ($0.00008\%^{-1}.s^{-1}$), for which the reaction slows down (Fig. 2b). Except for the U-EDTA system, only the U-NTA system seems to show a significant forward reaction between 5 s and 30 s with a reduction rate of $0.000\ 2\%^{-1}.s^{-1}$.

As described in the results section, we identified four behaviours across the U(VI)-ligand complexes based on reduction rates from 0 to 5s and from 5s to 30s: (1) slow for carbonate and hydroxo; (2) fast then slow for citrate; (3) fast then moderate for NTA; and (4) fast for EDTA.

Interestingly, the reduction rate for the U(VI)-NTA and U(VI)-EDTA complexes follows the trend observed with Fe(III)-NTA and Fe(III)-EDTA, but the rates are slower. Indeed, Wang *et al.* observed that MtrC MR-1 could reduce Fe(III)-$EDTA^-$ more rapidly than Fe(III)(OH)NTA^- (second order rate constant 0.7207 and $0.286\ \mu M^{-1}.s^{-1}$, respectively) (Wang *et al.*, 2008). This order in the reactivities with Fe(III)-ligand complexes EDTA > NTA was also observed by Ross *et al.* (2009) for MtrC, and for the purified undecaheme *c*-type cytochrome UndA (Shi *et al.*, 2011) for which the rate of reduction of Fe(III)-EDTA was about 100x more rapid than that of Fe(III)-NTA.

The substantial impact of speciation on the U(VI) reduction rate could arise from several possible mechanisms: (1) U-ligand complex stability could impact the reduction rate, as the thermodynamic barrier to reduction may be higher for high-stability complexes (Grenthe *et al.*, 1992; Palmer *et al.*, 2003; Hummel *et al.*, 2005, 2007); (2) ligand exchange kinetics could play a role if the complex dissociates prior to reduction; (3) steric hindrance due to the large size of some complexes could impair access to the protein site of electron transfer (Marcus and Sutin, 1985); and (4) differences in the electron transfer mechanism across U(VI)-ligand complexes could result in distinct reduction rates. Explanations (2) and (3) can be discarded because they are not supported by the data (EDTA has slow ligand exchange kinetics and is one of the largest complexes but has the highest reduction rate).

https://doi.org/10.1180/gbi.2024.10 Published online by Cambridge University Press

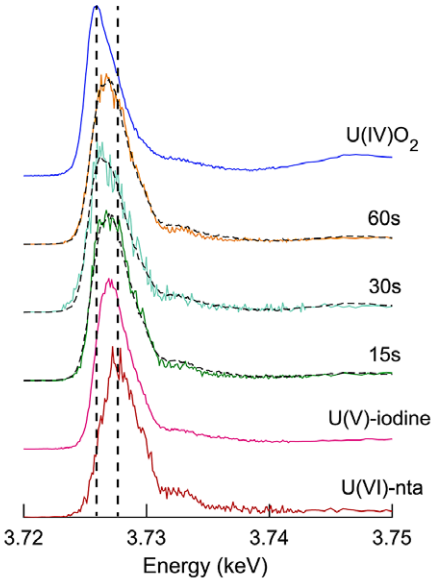

	% U(VI)	% U(V)	% U(IV)	R factor	Reduced χ^2
15s	19.65 ± 0.03	51.58 ± 0.03	28.76 ± 0.01	0.010	0.721
30s	10.75 ± 0.04	33.02 ± 0.05	56.23 ± 0.02	0.022	1.211
60s	14.59 ± 0.02	51.07 ± 0.03	34.34 ± 0.01	0.008	0.462

Figure 7. M_4-edge HR-XANES spectra of the reaction timeline between reduced MtrC baltica and U(VI)-NTA. The concentrations of reactants were: [U(VI)] = 600 μM and [MtrC baltica] = 300 μM in a buffer containing [NTA] = 30 mM, [NaCl] = 50 mM and [HEPES] = 100 mM at pH 7.5. Timepoints were taken after 15 s (dark green), 30 s (turquoise), 60 s (orange). The reference spectra used to interpret the data are U(VI)-NTA (red), U(V)-iodide (pink) and U(IV)O_2 (blue). The two dotted lines correspond to the whitelines of U(IV)O_2 on the left and that of U(VI)-carbonate on the right. Whitelines of the spectra are reported in Table S12.b. LCF fitting are displayed in dotted black line on the top of the M_4-edge HR-XANES spectra obtained. The fits were obtained by considering contributions from U(VI)-carbonate, U(V)-iodide and UO_2 (top panel) or contributions from U(VI)-nta, U(V)-iodine and U(IV)O_2 (bottom panel). Statistical parameters and results of the fit are summarized in the table below the figure.

There is no obvious correlation between U-complex stability and reaction rate

First, we consider the impact of the complex stability constant. The formation constants of the calculated dominant U(VI)-ligand complexes are ordered as follows: $\log K(U(VI)O_2(OH)_3^-) = -20.25 \pm 0.42$ (Palmer *et al.*, 2003) < $\log K(U(VI)O_2(OH)NTA^{2-}) = 2.39 \pm 0.04$ (De Stefano *et al.*, 2006) < $\log K(U(VI)O_2cit^-) = 8.96 \pm 0.11$ (Hummel *et al.*, 2007) < $\log K(U(VI)O_2EDTA^{2-}) = 13.7 \pm 0.2$ (Hummel *et al.*, 2007) < $\log K(U(VI)O_2(CO_3)_2^{2-}) = 16.94 \pm 0.12$ (Grenthe *et al.*, 1992) < $\log K((U(VI)O_2)_2cit_2^{2-}) = 21.3 \pm 0.3$ (Hummel *et al.*, 2007) < $\log K(U(VI)O_2(CO_3)_3^{4-}) = 21.60 \pm 0.05$ (Pashalidis *et al.*, 1997) (Table S9 and S10). Our initial hypothesis was that the greater the logK, the more stable the U(VI)-ligand complex and the slower the reduction by MtrC baltica. However, within the experimental condition set, the initial reaction rates were ordered as follows $k_{inital}(EDTA) > k_{initial}(NTA) > k_{inital}(citrate) >> k_{inital}(carbonate) \approx k_{inital}(hydroxo)$. Therefore, there is no obvious correlation between formation constant and reaction rate.

The reaction rate is related to the nature of interaction between U(VI)-complexes and MtrC

To probe the influence of the electron transfer mechanism on the reduction rates across the different U(VI)-ligand complexes, we first investigated the chemical interactions between the U(VI)-ligand complexes and MtrC baltica, which could explain the difference in reduction rates. Signals of the paramagnetic region of the NMR spectra (between 14 ppm and 35 ppm) illuminate the local chemistry around the hemes.

We attempted to attribute specific features of the MtrC baltica NMR spectrum to individual hemes, to help pinpoint the site of interaction. We used site-directed mutagenesis to replace one of the two axial histidines bound to the Fe centre of heme 2, 5, 7, 9 and 10 by a methionine, as previously done for OmcA (Neto *et al.*, 2017). We observed that for each mutant, a few peaks in the paramagnetic NMR spectra were affected (Fig. 3). This suggests that the overall protein structure is probably conserved with proper folding. In particular, we could attribute certain regions of the spectra to the studied mutated hemes, which narrows the interaction site possibilities. Probably the spectral region between 17 ppm and 20 ppm results from contribution of hemes 2, 5 and 10. The signal around 21.7 ppm and those around 23.51 ppm and 24.36 ppm are related to heme 5. The region between 30–34 ppm could represent signatures from hemes 2, 9 and 10. Interestingly, it is in regions attributed to heme 5 and 10 that most of the influences by ligands and U(VI)-ligand complexes were reported (Table 2). These two solvent exposed hemes are reported to function as an electron entrance (heme 5) and an electron exit (heme 10) when MtrC baltica is incorporated in the MtrCAB complex across the outer membrane of *S. baltica*. We expect a similar behaviour in MtrC MR-1, the structure of which resembles closely that of MtrC baltica with 46.6% of homology and identical positions of the hemes in the protein scaffold (Text S6 and Fig. S8). In bacterial cells, heme 5 is not solvent-exposed, hence no interaction with the electron acceptor is expected whereas here, with the purified protein, interaction with the substrate is possible.

Table 2. Summary of the main chemical shifts observed by NMR when oxidized MtrC baltica was reacted with the different U(VI)-ligand complexes (Fig. 4), and corresponding heme number based on the results presented (Fig. 3).

U(VI)-ligand complexes	Main chemical shifts (ppm)	Attributed heme
U(VI)-hydroxo	17.96	heme 10/2
	18.58	heme 10/5/2
	23.51	heme 5
	21.87	heme 10
U(VI)-carbonate	18.58	heme 10/5/2
	19.79	heme 10
	21.7	heme 5
	24.36	heme 5
U(VI)-citrate	17.96	heme 10/2
	18.58	heme 10/5/2
	21.7	heme 5
	24.36	heme 5
U(VI)-NTA	18.58	heme 10/5/2
	21.7	heme 5
	24.36	heme 5
U(VI)-EDTA	18.58	heme 10/5/2
	21.7	heme 5
	24.36	heme 5

https://doi.org/10.1180/gbi.2024.10 Published online by Cambridge University Press

We observed three principal types of behaviour in the interaction of MtrC baltica heme regions and U(VI)-ligand complexes. In the first type, the ligand alone has limited impact on the NMR signal, while the presence of the U(VI)-ligand complex results in clear shifts (Fig. 4). This was observed for U(VI)-hydroxo and U(VI)-carbonate. In the second type, the ligand impacts the NMR signal and addition of U(VI)-ligand enhanced this effect. This was the case for U(VI)-citrate. Finally, in the third case, the ligand itself has great impact on the NMR signal, and the addition of U(VI) does not induce further changes. This behaviour was observed for U(VI)-NTA and U(VI)-EDTA.

Interestingly, for U(VI)-carbonate and U(VI)-hydroxo which are reduced initially at a slower rate than the other U(VI)-ligand complexes (Fig. 1 and Fig. 2), the NMR signal is perturbed upon addition of U to the system (Fig. 4). This suggests that U(VI)-carbonate and U(VI)-hydroxo may interact with MtrC baltica (covalently or via hydrogen bonding) through the U atom in the vicinity of hemes 5 or 10, effectively shedding the ligand to bind the protein. This assumption is supported by the size-exclusion chromatography data, showing U bound to the protein in the U-carbonate case (Fig. 6 and Table S10). In addition, upon reduction of U(VI)-carbonate by MtrC MR1, 60.64% of U in the form of U(IV) remains bound to the protein (Fig S5.c and Tables S6 and S7). We infer that reduced U potentially precipitates around the terminal heme, which could slow down reaction progress.

Regarding U(VI)-EDTA and U(VI)-NTA, for which the most rapid kinetics are observed (Fig. 1 and Fig. 2), the NMR data suggest that the interaction occurs via the ligand (Fig. 4), thus the U-ligand complex remains intact. Finally, in the case of U(VI)-citrate, for which initial fast and then slow reduction rates were observed (Fig. 1 and Fig. 2), both the addition of citrate and U influenced the NMR signals (Fig. 4). Possibly, both the ligand and the U atom bind in the vicinity of hemes 5 or 10.

In the above-mentioned case, for citrate and NTA ligands, hydrogen bonds may form between the ligand and residues close to hemes 5 or 10 (Fig. 3). Indeed, Edwards *et al.* observed hydrogen bonds between citrate or NTA and the undecaheme *c*-type cytochrome UndA upon co-crystallization with Fe(III)-citrate and Fe(III)-NTA (Edwards *et al.,* 2012b). They observed that the Fe(III)-citrate trimer complex associates via hydrogen bonding to an arginine in the vicinity of heme 7. In addition, the Fe(III)-NTA dimer associates with UndA close to heme 7 via hydrogen bonding between a carboxylic group and the guanidinium group of an arginine and the backbone nitrogen of a serine and a lysine (Edwards *et al.,* 2012b).

Regarding the EDTA system, the NMR results are comparable to those of NTA, although U(VI)-EDTA reduction displays a faster reduction rate. We cannot exclude that U(VI)-EDTA could bind through the ligand via hydrogen bonds, as suggested for U(VI)-NTA and U(VI)-citrate. However, in Edwards *et al.*'s work, Fe(III)-EDTA could not be co-crystallized with UndA (Edwards *et al.,* 2012b), unlike Fe(III)-citrate and Fe(III)-NTA. Therefore, the authors concluded that a weaker interaction could take place with UndA residues, such as electrostatic interaction. We could extend these results to the observed fast reduction rate of U(VI)-EDTA by MtrC where electrostatically interaction via the ligand could take place and allow rapid electron hopping.

Moreover, for organic ligands such as citrate, NTA, and EDTA, the reaction progression is probably facilitated by favourable complexation constants of the U(IV) products (Table S10). Indeed, the logK values of U(IV)-citrate, U(IV)-NTA and U(IV)-EDTA are high: 19.46 for $U(IV)(cit)_2^{2-}$, 15.6 ± 0.8 for U(IV)-NTA, 28.6 ± 1.6 for U(IV)-NTA_2 and 29.5 ± 0.2 for U(IV)-EDTA(aq). Furthermore, the presence of strong organic ligands such as NTA and EDTA inhibited the precipitation of U(IV) after reduction of U(VI)-NTA and U(VI)-EDTA by MtrC MR-1 (Fig. S5.b and S5.c, Table S6 and S7), confirming previously reported results (Ganesh *et al.,* 1997; Haas and Northup, 2004; Suzuki *et al.,* 2010), probably due to their high logK values (Table S10).

Role of U(V) in the mechanism of interaction between MtrC and U-ligand complexes

In addition, the formation of a stabilized U(V) intermediate may contribute to slowing down the reduction reaction. The role of U(V) was investigated by M_4-edge HR-XANES spectroscopy, which allowed us to resolve the U oxidation state in reactions between reduced MtrC and U(VI)-ligand complexes.

For carbonate, M_4-edge HR-XANES data evidence the formation and persistence of U(V) in association with the protein (Fig. 5). This U(V) intermediate must have a close interaction with MtrC otherwise, it would spontaneously disproportionate in carbonate buffer at pH 7.5 (Kern and Orlemann, 1949). Moreover, we showed that U(IV) formed upon reduction of U(VI)-carbonate remains associated with MtrC (Fig S5.c).

Regarding U(VI)-NTA, the M_4-edge HR-XANES data suggest the potential formation of U(V) in the first minutes of the reaction (Fig. 7, and Fig. S13) but not its persistence (Table S14). As for the U(VI)-EDTA data set, although it is noisier than that of U(VI)-carbonate or U(VI)-NTA, transient formation of a U(V) intermediate is not excluded (Fig. S12 and Fig. S14). Therefore, the reduction of the aminocarboxylate complexes U(VI)-NTA and U(VI)-EDTA could proceed as previously described for the aminocarboxylate complex U(VI)-dpaea, for which two successive one electron transfers occur (Molinas *et al.,* 2021, 2023).

Proposed mechanism of electron transfer from MtrC baltica to U(VI)-ligand complexes

As summarized in Fig. 8, we propose three distinct mechanisms of U(VI) reduction by MtrC, depending on the ligand. This model emerges from the four distinct reduction kinetics reported here, combined with the three types of behaviours observed by NMR spectroscopy, and taking into consideration previous studies (Edwards *et al.,* 2012b).

In the case of U(VI)-carbonate or U(VI)-hydroxo complexes, exhibiting slower reduction rates, we propose that covalent bonding to the U atom to a site in the vicinity of a terminal heme occurs, as reported by Sundararajan *et al.* (Sundararajan *et al.,* 2008). However, we cannot decipher whether, over time, the reduction is slowed down or the reduction process is inhibited due to the accumulation of reduced solid U species in close vicinity of the electron transfer sites.

Regarding U(VI)-NTA, the rapid initial reduction rates stem form weaker interaction with MtrC involving the ligand. We posit that U(VI)-NTA can approach a terminal heme via hydrogen bonding, as reported for Fe(III)-citrate and Fe(III)-NTA (Edwards *et al.,* 2012b). Two electrons can be transferred from the terminal heme to the U complexes, following the mechanism described for U(VI)-dpaea (Molinas *et al.,* 2021) and the formation of transient U(V). The reduced form of U remains complexed due to its affinity to the same ligands, resulting in soluble complexed U(IV).

https://doi.org/10.1180/gbi.2024.10 Published online by Cambridge University Press

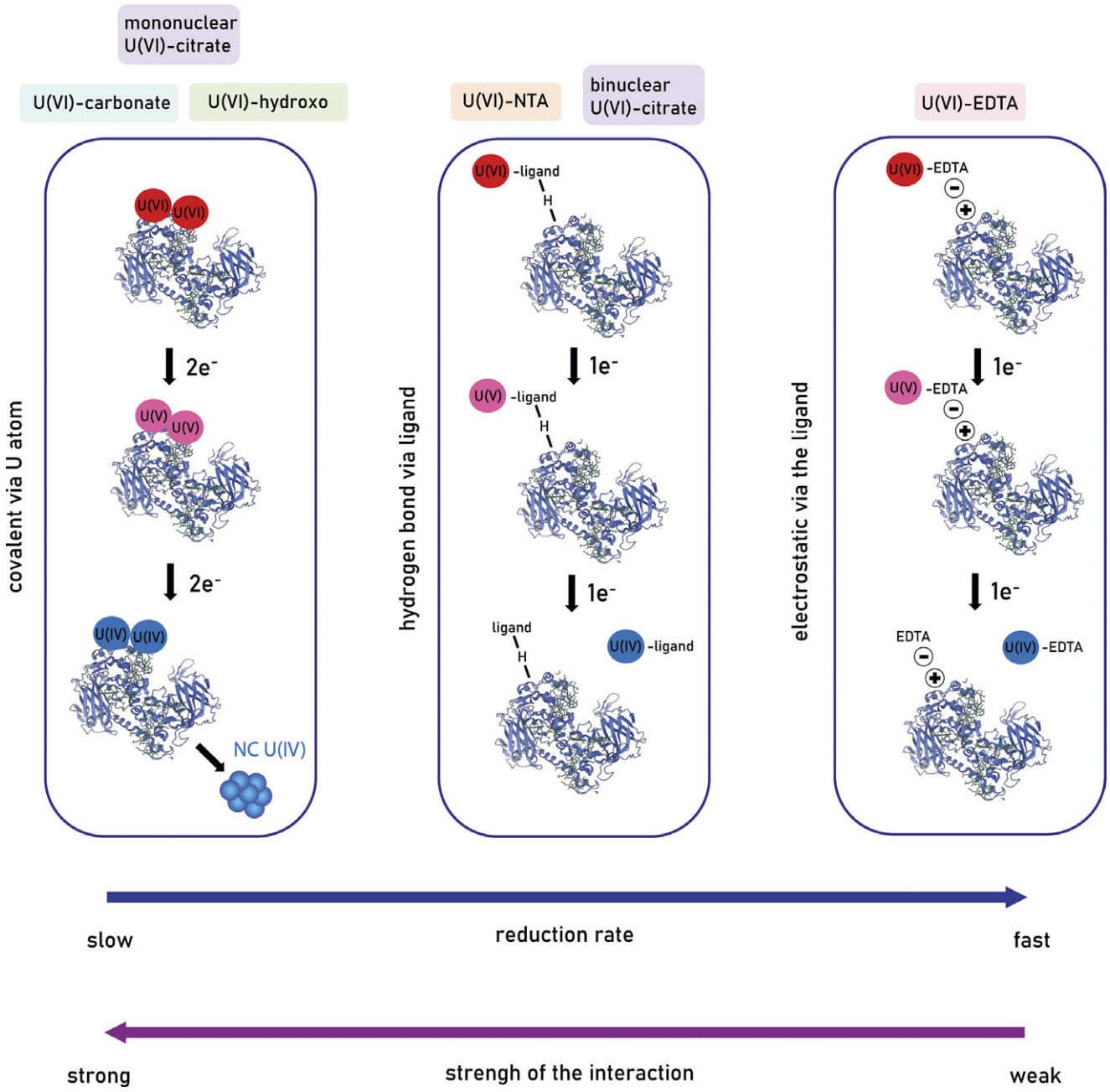

Figure 8. Summary of the observed factors which could regulate electron transfer rate between reduced MtrC baltica and the U(VI)-ligands complexes studied in this work. For U(VI)-carbonate and U(VI)-hydroxo, slow reduction rates were observed and are attributed to a stronger interaction with the reduction site of the protein, promoting potential covalent bonding. Stabilization of the U(V) intermediate could also lead to a decrease in the overall reduction rate. As for U(VI)-NTA, the interaction with the MtrC reduction site occurs with hydrogen bonding via the NTA ligand. For U(VI)-EDTA, for which the fastest reduction rates were observed, electrostatic interaction could take place allowing rapid electron hoping. For U(VI)-citrate, possibly two mechanisms are observed depending on the speciation. We propose that the mononuclear complex behaves as U(VI)-carbonate and U(VI)-hydroxo, with a covalent interaction between the U atom and residues of MtrC around the terminal heme; whereas the binuclear complex behaves as U(VI)-NTA, for which interaction probably occur via hydrogen bonding of the ligand to MtrC. In addition, the presence of the strong organic ligands citrate, NTA, or EDTA allows for rapid removal of the U(IV) product from the reduction site. The MtrC baltica (6QYC) structure was fetched from the Protein Data Bank (PDB).

As for U(VI)-EDTA, which displays the fastest overall reduction rate, we propose that the ligand interacts electrostatically with residues in the vicinity of the terminal heme, as previously suggested (Edwards *et al.,* 2012b), allowing two successive electrons to hop to U(VI).

Interestingly, U(VI)-citrate displayed a rapid initial reduction rate, which slowed down and behaved then similarly to that of U(VI)-carbonate and U(VI)-hydroxo complexes between 5s and 30s of reaction. In addition, the NMR signal indicated an impact from the addition of U in this system. We propose that U(VI)-citrate can bind residues around the terminal heme through hydrogen bonds via the ligand, but also via the U atom, namely for the mononuclear U(VI)-citrate complex, UO_2cit, for which the U atom is accessible in the equatorial plane. We propose that the binuclear complex, $(UO_2)_2cit_2^{2-}$ interacts exclusively via the ligand as the U atoms are shielded by the two ligands.

https://doi.org/10.1180/gbi.2024.10 Published online by Cambridge University Press

Conclusion

U(VI)-ligand complexes show varying modes of interaction with MtrC

In this study, we investigated the parameters which may influence the reduction rate of U(VI) by purified *c*-type cytochrome MtrC from two *Shewanella* species. We first concluded that the reduction mechanism is highly dependent on speciation. We observed that reaction rates were grouped in two clusters, one with more rapid initial rates observed with U(VI)-citrate, U(VI)-NTA and U(VI)-EDTA, and one with slower rates, comprising U(VI)-carbonate and U(VI)-hydroxo. Clearly, the hypothesis of a correlation between logK and reduction rates does not hold here, since U(VI)-EDTA was reduced more rapidly and has one of the higher logK of the series. However, we propose that the nature of the interaction, the persistence of the U(V) intermediate and the aqueous chemistry of the U(IV) species control the electron transfer rate. We propose that hydrogen bonds may form between U(VI)-citrate, U(VI)-NTA or U(VI)-EDTA complexes and MtrC baltica, whereas, covalent bonding between the U atom and MtrC baltica governs interactions with U(VI)-carbonate or U(VI)-hydroxo.

Limits of the experimental study and outlook

We chose to work with purified MtrC and performed enzymatic assays between MtrC and soluble U complexes. This system allows us to study specifically the interaction between two molecules; however, the experimental conditions are far from *in vivo* conditions, under which the protein receives a continuous flow of electrons when embedded within the outer membrane of bacterial cells. Hence, MtrC may display distinct redox potentials and redox properties when isolated or when embedded in the outer membrane. In addition, several electron exits may be available and energetically accessible in the isolated MtrC, as there are four solvent-exposed hemes in the structure of MtrC hemes 2 and 7, and hemes 5 and 10 (Edwards *et al.,* 2015). These are probably not as readily accessible in the membrane-associated protein. Moreover, we lack information on thermodynamic parameters, namely the redox potential of the selected U complexes, for U(VI)/U(V) and the U(V)/U(IV) redox couples. These would allow us to estimate the free energy of the redox reactions between the U-ligand complexes and the terminal hemes. The redox potential of the terminal hemes is already known for MtrF, a homologue of MtrC (Breuer *et al.,* 2012; Edwards *et al.,* 2017).

Future studies should target the binding strength, namely by investigating the crystallization of the four U-complexes with MtrC in order to identify binding regions of U soluble substrates, but also the nature of their interaction with MtrC. Alternative methods include Atomic Force Microscopy (AFM) to probe the strength of interaction between the U-complexes and MtrC, or investigating engineered proteins lacking terminal hemes or electrostatically altered putative hydrogen bonding regions to better grasp the mechanism of electron transfer.

Supplementary material. The supplementary material for this article can be found at http://doi.org/10.1180/gbi.2024.10.

Acknowledgements. We acknowledge the KIT light source for the infrastructure and we would like to thank the Institute for Beam Physics and Technology (IBPT) for the operation of the storage ring, the Karlsruhe Research Accelerator (KARA). We acknowledge also Dr Jörg Rothe and Dr Kathy Dardenne for their help with the organization of the synchrotron experiments. We thank the Protein Production and Structure Core Facility at EPFL, in particular Dr Florence Pojer, Dr Kelvin Lau and Amédé Larabi, for supporting us in the production and purification of both MtrC MR-1 and MtrC baltica. We thank Dr Marcus Edwards for providing us with the soluble MtrC baltica construct and collaborating through fruitful discussions.

Author Contribution. The manuscript was written through contributions from all authors. RBL conceived the research. MM performed all the experiments with support from KM for the proper workflow of site-directed mutagenesis, LAA who designed and carried out the NMR experiments, AB who developed the ion-exchange chromatography method, and TP who assisted with the HR-XANES measurements. All authors gave approval for the final version of the manuscript.

Funding Sources. This research was supported financially by the Swiss National Science Foundation (SNSF) with project numbers CR23I2_166455 and 200021E-164209 and by the European Research Council Consolidator Grant 725675 (UNEARTH).

Financial Interests. The authors declare no competing financial interest.

References

Bargar J.R., Bernier-Latmani R., Giammar D.E. and Tebo B.M. (2008) Biogenic uraninite nanoparticles and their importance for uranium remediation. *Elements*, **4**, 407–412, https://doi.org/10.2113/gselements.4.6.407.

Bernier-Latmani R., Veeramani H., Dalla Vecchia E., Junier P., Lezama-Pacheco J.S., Suvorova E.I., Sharp J.O., Wigginton N.S., and Bargar J.R., (2010) Non-uraninite products of microbial U(VI) reduction. *Environmental Science & Technology*, **44**, 9456–9462, https://doi.org/10.1021/es101675a.

Breuer M., Zarzycki P., Blumberger J. and Rosso K.M. (2012) Thermodynamics of Electron Flow in the Bacterial Deca-heme Cytochrome MtrF. *Journal of the American Chemical Society*, **134**, 9868–9871, https://doi.org/10.1021/ja3027696.

Breuer M., Rosso K.M. and Blumberger J. (2014) Electron flow in multiheme bacterial cytochromes is a balancing act between heme electronic interaction and redox potentials. *Proceedings of the National Academy of Sciences of the United States of America*, **111**, 611–616, https://doi.org/10.1073/pnas.1316156111.

Brown A.R., Molinas M., Roebbert Y., Sato A., Abe M., Weyer S. and Bernier-Latmani R. (2023) Electron flux is a key determinant of uranium isotope fractionation during bacterial reduction. *Communications Earth & Environment*, **4**, 1–11, https://doi.org/10.1038/s43247-023-00989-x.

De Stefano C., Gianguzza A., Milea D., Pettignano A. and Sammartano S. (2006) Sequestering ability of polyaminopolycarboxylic ligands towards dioxouranium(VI) cation. *Journal of Alloys and Compounds*, **424**, 93–104, https://doi.org/10.1016/j.jallcom.2006.01.003.

Edwards M.J., Fredrickson J.K., Zachara J.M., Richardson D.J. and Clarke T.A. (2012a) Analysis of structural MtrC models based on homology with the crystal structure of MtrF. *Biochemical Society Transactions*, **40**, 1181–1185, https://doi.org/10.1042/BST20120132.

Edwards M.J., Hall A., Shi L., Fredrickson J.K., Zachara J.M., Butt J.N., Richardson D.J., and Clarke T.A. (2012b) The Crystal Structure of the Extracellular 11-heme Cytochrome UndA Reveals a Conserved 10-heme Motif and Defined Binding Site for Soluble Iron Chelates. *Structure*, **20**, 1275–1284, https://doi.org/10.1016/j.str.2012.04.016.

Edwards M.J., White G.F., Norman M., Tome-Fernandez A., Ainsworth E., Shi L., Fredrickson J.K., Zachara J.M., Butt J.M., Richardson D.J., and Clarke T.A. (2015) Redox Linked Flavin Sites in Extracellular Decaheme Proteins Involved in Microbe-Mineral Electron Transfer. *Scientific Reports*, **5**, 11677, https://doi.org/10.1038/srep11677.

Edwards M.J., Gates A.J., Butt J.N., Richardson D.J. and Clarke T.A. (2017) Comparative structure-potentio-spectroscopy of the Shewanella outer membrane multiheme cytochromes. *Current Opinion in Electrochemistry*, **4**, 199–205, https://doi.org/10.1016/j.coelec.2017.08.013.

Edwards M.J., White G.F., Butt J.N., Richardson D.J. and Clarke T.A. (2020) The Crystal Structure of a Biological Insulated Transmembrane Molecular Wire. *Cell*, **181**, 665–673. e10, https://doi.org/10.1016/j.cell.2020.03.032.

Ferreira M.R. and Salgueiro C.A. (2018) Biomolecular Interaction Studies Between Cytochrome PpcA From Geobacter sulfurreducens and the Electron

Acceptor Ferric Nitrilotriacetate (Fe-NTA). *Frontiers in Microbiology*, **9**, 2741.

Francis A.J., Dodge C.J., Lu Fulong., Halada G.P. and Clayton C.R. (1994) XPS and XANES Studies of Uranium Reduction by Clostridium sp. *Environmental Science & Technology*, **28**, 636–639, https://doi.org/10.1021/es00053a016.

Fukushima T., Gupta S., Rad B., Cornejo J.A., Petzold C.J., Chan L.J.G., Mizrahi R.A., Ralsto C.Y. and Ajo-Franklin C.M. (2017) The Molecular Basis for Binding of an Electron Transfer Protein to a Metal Oxide Surface. *Journal of the American Chemical Society*, **139**, 12647–12654, https://doi.org/10.1021/jacs.7b06560.

Ganesh R., Robinson K.G., Reed G.D. and Sayler G.S. (1997) Reduction of hexavalent uranium from organic complexes by sulfate- and iron-reducing bacteria. *Applied Environmental Microbiology*, **63**, 4385–4391.

Grenthe I., Fuger J., Lemire R.J., Muller A.B., Nguyen-Trung Cregu C. and Wanner H. (1992) *Chemical thermodynamics of uranium*. Elsevier, Amsterdam, Netherlands.

Haas J.R. and Northup A. (2004) Effects of aqueous complexation on reductive precipitation of uranium by Shewanella putrefaciens. *Geochemical Transactions*, **5**, 41, 1467–4866, https://doi.org/10.1186/1467-4866-5-41.

Hartshorne R.S., Reardon C.L., Ross D., Nuester J., Clarke T.A., Gates A.J., Mills P.C., Fredrickson J.K., Zachara J.M., Shi L., Beliaev A.S., Marshall M.J., Tien M., Brantley S., Butt J.N., and Richardson D.J. (2009) Characterization of an electron conduit between bacteria and the extracellular environment. *Proceedings of the National Academy of Sciences of the United States of America*, **106**, 22169–22174, https://doi.org/10.1073/pnas.0900086106.

Hummel W., Anderegg G., Rao L., Puigdomenech I. and Tochiyama O. (2005) *Chemical Thermodynamics of Compounds and Complexes of U, Np, Pu, Am, Tc, Se, Ni and Zr with Selected Organic Ligands*. OECD Publishing, Paris.

Hummel W., Puigdomènech I., Rao L. and Tochiyama O. (2007) Thermodynamic data of compounds and complexes of U, Np, Pu and Am with selected organic ligands. *Comptes Rendus Chimie*, **10**, 948–958, https://doi.org/10.1016/j.crci.2007.03.012.

Kern D.M.H. and Orlemann E.F. (1949) The Potential of the Uranium (V), Uranium (VI) Couple and the Kinetics of Uranium (V) Disproportionation in Perchlorate Media. *Journal of the American Chemical Society*, **71**, 2102–2106, https://doi.org/10.1021/ja01174a055.

Lovley D.R., Phillips E.J.P., Gorby Y.A. and Landa E.R. (1991) Microbial reduction of uranium. *Nature*, **350**, 413–416, https://doi.org/10.1038/350413a0.

Lovley D.R., Roden E.E., Phillips E.J.P. and Woodward J.C. (1993) Enzymatic iron and uranium reduction by sulfate-reducing bacteria. *Marine Geology*, **113**, 13.

Lower B.H., Shi L., Yongsunthon R., Droubay T.C., McCready D.E. and Lower S.K. (2007) Specific bonds between an iron oxide surface and outer membrane cytochromes MtrC and OmcA from Shewanella oneidensis MR-1. *Journal of Bacteriology*, **189**, 4944–4952, https://doi.org/10.1128/JB.01518-06.

Marcus R.A. and Sutin N. (1985) Electron transfers in chemistry and biology. *Biochimica et Biophysica Acta (BBA) - Reviews on Bioenergetics*, **811**, 265–322, https://doi.org/10.1016/0304-4173(85)90014-X.

Marshall M.J., Beliaev A.S., Dohnalkova A.C., Kennedy D.W., Shi L., and Wang Z. (2006) c-Type Cytochrome-Dependent Formation of U(IV) Nanoparticles by Shewanella oneidensis. *PLoS Biology*, **4**(8), e268. https://doi.org/10.1371/journal.pbio.0040268.

Molinas M., Faizova R., Brown A., Galanzew J., Schacherl B., Bartova B., Meibom K.L., Vitova T., Mazzanti M., and Bernier-Latmani R. (2021) Biological Reduction of a U(V)–Organic Ligand Complex. *Environmental Science & Technology*, **55**, 4753–4761, https://doi.org/10.1021/acs.est.0c06633.

Molinas M., Meibom K.L., Faizova R., Mazzanti M. and Bernier-Latmani R. (2023) Mechanism of Reduction of Aqueous U(V)-dpaea and Solid-Phase U(VI)-dpaea Complexes: The Role of Multiheme c-Type Cytochromes. *Environmental Science & Technology*, **57**(19), 7537–7546, https://doi.org/10.1021/acs.est.3c00666.

Neto S.E., de Melo-Diogo D., Correia I.J., Paquete C.M. and Louro R.O. (2017) Characterization of OmcA Mutants from Shewanella oneidensis MR-1 to Investigate the Molecular Mechanisms Underpinning Electron Transfer Across the Microbe-Electrode Interface. *Fuel Cells*, **17**, 601–611, https://doi.org/10.1002/fuce.201700023.

O'Loughlin E.J., Kelly S.D., Cook R.E., Csencsits R. and Kemner K.M. (2003) Reduction of Uranium(VI) by Mixed Iron(II)/Iron(III) Hydroxide (Green Rust): Formation of UO2 Nanoparticles. *Environmental Science & Technology*, **37**, 721–727, https://doi.org/10.1021/es0208409.

Palmer D., Guillaumont R., Fanghaenel T., Neck V., Fuger J., Grenthe I. and Rand M. (2003) Chemical Thermodynamics Vol. 5 : Update on the Chemical Thermodynamics of Uranium, Neptunium, Plutonium, Americium, and Technetium. OECD Publishing, Paris.

Paquete C.M., Fonseca B.M., Cruz D.R., Pereira T.M., Pacheco I., Soares C.M. and Louro R.O. (2014) Exploring the molecular mechanisms of electron shuttling across the microbe/metal space. *Frontiers in Microbiology*, **5**, 318, https://doi.org/10.3389/fmicb.2014.00318.

Pashalidis I., Czerwinski K.R., Fanghänel T. and Kim J.I. (1997) Solid-Liquid Phase Equilibria of Pu(VI) and U(VI) in Aqueous Carbonate Systems. *Determination of Stability Constants*. Radiochimica Acta, **76**, 55–62, https://doi.org/10.1524/ract.1997.76.12.55.

Pirbadian S. and El-Naggar M.Y. (2012) Multistep hopping and extracellular charge transfer in microbial redox chains. *Physical Chemistry Chemical Physics*, **14**, 13802–13808, https://doi.org/10.1039/C2CP41185G.

Ravel B. and Newville M. (2005) ATHENA, ARTEMIS, HEPHAESTUS: data analysis for X-ray absorption spectroscopy using IFEFFIT. *Journal of Synchrotron Radiation*, **12**, 537–541, https://doi.org/10.1107/S0909049505012719.

Richardson D.J., Edwards M.J., White G.F., Baiden N., Hartshorne R.S., Fredrickson J., Shi L., Zachara J., Gates A.J., Butt J.N., and Clarke T.A. (2012) Exploring the biochemistry at the extracellular redox frontier of bacterial mineral Fe(III) respiration. *Biochemical Society Transactions*, **40**, 493–500, https://doi.org/10.1042/BST20120018.

Ross D.E., Ruebush S.S., Brantley S.L., Hartshorne R.S., Clarke T.A., Richardson D.J. and Tien M. (2007) Characterization of Protein-Protein Interactions Involved in Iron Reduction by Shewanella oneidensis MR-1. *Applied and Environmental Microbiology*, **73**, 5797–5808, https://doi.org/10.1128/AEM.00146-07.

Ross D.E., Brantley S.L. and Tien M. (2009) Kinetic Characterization of OmcA and MtrC, Terminal Reductases Involved in Respiratory Electron Transfer for Dissimilatory Iron Reduction in Shewanella oneidensis MR-1. *Applied and Environmental Microbiology*, **75**, 5218–5226, https://doi.org/10.1128/AEM.00544-09.

Schuetz B., Schicklberger M., Kuermann J., Spormann A.M. and Gescher J. (2009) Periplasmic Electron Transfer via the c-Type Cytochromes MtrA and FccA of Shewanella oneidensis MR-1. *Applied and Environmental Microbiology*, **75**, 7789–7796, https://doi.org/10.1128/AEM.01834-09.

Schwalb C., Chapman S.K. and Reid G.A. (2002) The membrane-bound tetrahaem c-type cytochrome CymA interacts directly with the soluble fumarate reductase in Shewanella. *Biochemical Society Transactions*, **30**, 658–662, https://doi.org/10.1042/bst0300658.

Scott T.B., Allen G.C., Heard P.J. and Randell M.G. (2005) Reduction of U(VI) to U(IV) on the surface of magnetite. *Geochimica et Cosmochimica Acta*, **69**, 5639–5646, https://doi.org/10.1016/j.gca.2005.07.003.

Shi L., Chen B., Wang Z., Elias D.A., Mayer M.U., Gorby Y.A., Ni S., Lower B.H., Kennedy D.W., Wunschel D.S., Mottaz H.M., Marshall M.J., Hill E.A., Beliaev A.S., Zachara J.M., Fredrickson J.K., and Squier T.C. (2006) Isolation of a High-Affinity Functional Protein Complex between OmcA and MtrC: Two Outer Membrane Decaheme c-Type Cytochromes of Shewanella oneidensis MR-1. *Journal of Bacteriology*, **188**, 4705–4714, https://doi.org/10.1128/JB.01966-05.

Shi L., Belchik S.M.,Wang Z., Kennedy D.W., Dohnalkova A.C., Marshall M.J., Zachara J.M., and Fredrickson J.K. (2011) Identification and Characterization of UndAHRCR-6, an Outer Membrane Endecaheme c-Type Cytochrome of Shewanella sp. Strain HRCR-6. *Applied and Environmental Microbiology*, **77**, 5521–5523, https://doi.org/10.1128/AEM.00614-11.

Sundararajan M., Campbell A.J. and Hillier I.H. (2008) Catalytic cycles for the reduction of [UO2]2+ by cytochrome c7 proteins proposed from DFT calculations. *The Journal of Physical Chemistry. A*, **112**, 4451–4457, https://doi.org/10.1021/jp800209p.

Suzuki Y., Tanaka K., Kozai N. and Ohnuki T. (2010) Effects of Citrate, NTA, and EDTA on the Reduction of U(VI) by Shewanella putrefaciens. *Geomicrobiology Journal*, **27**, 245–250, https://doi.org/10.1080/01490450903456764.

Tandy S., Bossart K., Mueller R., Ritschel J., Hauser L., Schulin R. and Nowack B. (2004) Extraction of Heavy Metals from Soils Using Biodegradable Chelating

Agents. *Environmental Science & Technology*, **38**, 937–944, https://doi.org/10.1021/es0348750.

Veeramani H. and Scheinost A.C.(2013) Abiotic Reductive Immobilization of U(VI) by Biogenic Mackinawite. *Environmental Science & Technology*, **47**, 2361–2369, https://doi.org/10.1021/es304025x.

Veeramani H., Alessi D.S., Suvorova E.I., Lezama-Pacheco J.S., Stubbs J.E., Sharp J.O., Dippon U., Kappler A., Bargar J.R., and Bernier-Latmani R. (2011) Products of abiotic U(VI) reduction by biogenic magnetite and vivianite. *Geochimica et Cosmochimica Acta*, **75**, 2512–2528, https://doi.org/10.1016/j.gca.2011.02.024.

Wang Z., Liu C., Wang X., Marshall M.J., Zachara J.M., Rosso K.M., Dupuis M., Fredrickson J.K., Heald S., and Shi L., (2008) Kinetics of reduction of Fe(III) complexes by outer membrane cytochromes MtrC and OmcA of Shewanella oneidensis MR-1. *Applied and Environmental Microbiology*, **74**, 6746–6755, https://doi.org/10.1128/AEM.01454-08.

Watanabe H.C., Yamashita Y. and Ishikita H. (2017) Electron transfer pathways in a multiheme cytochrome MtrF. *Proceedings of the National Academy of Sciences*, **114**, 2916–2921, https://doi.org/10.1073/pnas.1617615114.

White G.F., Shi Z., Shi L., Wang Z., Dohnalkova A.C., Marshall M.J., Fredrickson J.K., Zachara J.M., Butt J.M., Richardson D.J., and Clarke T.A., (2013) Rapid electron exchange between surface-exposed bacterial cytochromes and Fe(III) minerals. *Proceedings of the National Academy of Sciences*, **110**, 6346–6351, https://doi.org/10.1073/pnas.1220074110.

Wigginton N.S., Rosso K.M., Lower B.H., Shi L. and Hochella M.F. (2007a) Electron tunneling properties of outer-membrane decaheme cytochromes from Shewanella oneidensis. *Geochimica et Cosmochimica Acta*, **71**, 543–555, https://doi.org/10.1016/j.gca.2006.10.002.

Wigginton N.S., Rosso K.M. and Hochella M.F. (2007b) Mechanisms of Electron Transfer in Two Decaheme Cytochromes from a Metal-Reducing Bacterium. *The Journal of Physical Chemistry B*, **111**, 12857–12864, https://doi.org/10.1021/jp0718698.

Zimina A., Dardenne K., Denecke M.A., Doronkin D.E., Huttel E., Lichtenberg H., Mangold S., Pruessmann T., Rothe J., Spangenberg T., Steininger R., Vitova T., Geckeis H. and Grunwaldt J.D. (2017) CAT-ACT—A new highly versatile x-ray spectroscopy beamline for catalysis and radionuclide science at the KIT synchrotron light facility ANKA. *Review of Scientific Instruments*, 88, 113113, https://doi.org/10.1063/1.4999928.

https://doi.org/10.1180/gbi.2024.10 Published online by Cambridge University Press